The influence of the secondary electrons induced by energetic electrons impacting the Cassini Langmuir probe at Saturn

P. Garnier,[1,2] M. K. G. Holmberg,[3] J.-E. Wahlund,[3] G. R. Lewis,[4,5] S. Rochel Grimald,[1,2,6] M. F. Thomsen,[7] D. A. Gurnett,[8] A. J. Coates,[4,5] F. J. Crary,[9] and I. Dandouras[1,2]

[1]   The Cassini Langmuir Probe (LP) onboard the Radio and Plasma Wave Science experiment has provided much information about the Saturnian cold plasma environment since the Saturn Orbit Insertion in 2004. A recent analysis revealed that the LP is also sensitive to the energetic electrons (250–450 eV) for negative potentials. These electrons impact the surface of the probe and generate a current of secondary electrons, inducing an energetic contribution to the DC level of the current-voltage (I-V) curve measured by the LP. In this paper, we further investigated this influence of the energetic electrons and (1) showed how the secondary electrons impact not only the DC level but also the slope of the (I-V) curve with unexpected positive values of the slope, (2) explained how the slope of the (I-V) curve can be used to identify where the influence of the energetic electrons is strong, (3) showed that this influence may be interpreted in terms of the critical and anticritical temperatures concept detailed by Lai and Tautz (2008), thus providing the first observational evidence for the existence of the anticritical temperature, (4) derived estimations of the maximum secondary yield value for the LP surface without using laboratory measurements, and (5) showed how to model the energetic contributions to the DC level and slope of the (I-V) curve via several methods (empirically and theoretically). This work will allow, for the whole Cassini mission, to clean the measurements influenced by such electrons. Furthermore, the understanding of this influence may be used for other missions using Langmuir probes, such as the future missions Jupiter Icy Moons Explorer at Jupiter, BepiColombo at Mercury, Rosetta at the comet Churyumov-Gerasimenko, and even the probes onboard spacecrafts in the Earth magnetosphere.

1. Introduction

[2]   The Langmuir probe—referred to as LP in the paper—onboard the Cassini spacecraft is part of the Radio and Plasma Wave Science (RPWS) instrument [*Gurnett et al.*, 2004]. It has brought much information about the cold and dense plasma in the Saturnian system since 2004, in par-ticular regarding the Titan ionosphere [e.g., *Wahlund et al.*, 2005a; *Ågren et al.*, 2007; *Garnier et al.*, 2009; *Edberg et al.*, 2011]. The LP also allowed to study the Saturnian plasma disk [*Wahlund et al.*, 2005b; *Morooka et al.*, 2009; *Gustafsson and Wahlund*, 2010] or dusty regions such as the Enceladus plume or the rings environment [*Wahlund et al.*, 2009; *Morooka et al.*, 2011].

[3]   The LP is dedicated to the investigation of cold (below electron temperatures of $\sim$ 5 eV) and dense (above several particles per cubic centimeter) plasmas. *Garnier et al.* [2012b], however, also revealed a strong sensitivity of the LP measurements to the energetic electrons (the adjective "energetic" will refer to energies around $\sim$ 250–450 eV in this paper). The analysis of the ion side current (current for negative potentials) measured by the probe showed indeed a correlation with these energetic electrons, which impact the surface of the LP and generate a detectable current of secondary electrons. The spatial distribution of the 250–450 eV electrons in the magnetosphere [*DeJong et al.*, 2011] then lead *Garnier et al.* [2012b] to observe a broad secondary electron current region in the dipole L shell range of $\sim$ 6–10.

[1]Université de Toulouse; UPS-OMP; IRAP; Toulouse, France.
[2]CNRS; IRAP, Toulouse, France.
[3]Swedish Institute of Space Physics, Uppsala, Sweden.
[4]Mullard Space Science Laboratory, University College London, Dorking, UK.
[5]The Centre for Planetary Sciences at UCL/Birkbeck, London, UK.
[6]Onera-The French Aerospace Lab, Toulouse, France.
[7]Planetary Science Institute, Tucson, Arizona, USA.
[8]Department of Physics and Astronomy, University of Iowa, Iowa City, Iowa, USA.
[9]Laboratory for Atmospheric and Space Physics, University of Colorado, Boulder, Colorado, USA.

Corresponding author: P. Garnier, IRAP, 9, avenue du Colonel Roche, BP 44346, 31028 Toulouse cedex 4, France. (Philippe.Garnier@irap.omp.eu)

[4] The purpose of our study is to understand in more detail why this current exists and how we can model it. This will allow either to infer valuable information about the plasma or to remove this current from the measurements (it may be considered as a parasite current for the cold plasma investigations). *Garnier et al.* [2012b, hereinafter G12] indeed identified the source particles of the measured current through a correlation analysis but did not reproduce the current itself. Moreover, the authors focused only on the contribution by the energetic particles on the DC level of the current-voltage curve of the LP (the so called I_{ener} current). We will, however, show here that the energetic particles also impact the slope of this curve by adding a contribution b_{ener}.

[5] The paper is organized as follows: section 2 will describe the instruments and data sets used in our study; section 3 will focus on the slope of the current-voltage curve measured by the LP and its interpretation; sections 4 and 5 will then describe two different methods (respectively, empirical and theoretical) to model the impact of the energetic electrons (both I_{ener} and b_{ener} contributions); a comparative discussion on the various modeling methods will be given in section 6; a summary will end the paper in section 7, followed by an Appendix A with the derivation of the equations used.

2. Description of the Data

[6] This section will first present the time intervals used in our study (section 2.1). It will then describe the data used from the LP experiment (section 2.2; see *Gurnett et al.* [2004] for a description of the LP) and from the CAPS (Cassini Plasma Spectrometer) experiment (section 2.3; see *Young et al.* [2004] for a description of CAPS). The time intervals used here are identical to those discussed in G12; we thus also refer the reader to sections 2 and 3 of G12 for detailed explanations.

2.1. Description of the Time Intervals Used

[7] The time intervals chosen in this paper correspond to the two types of studies presented here: event analysis and statistical study over several years of data. The data sets were chosen to focus on regions where the influence of the energetic electrons is the strongest, but one should keep in mind that this influence may be seen in a large part of the magnetosphere. We will first present the event data set and then the statistical study one.

[8] The case studies chosen include the inbound part of the SOI (Saturn Orbit Insertion) in 2004 and a high-inclination orbit in 2008. During the inbound part of SOI (30 June 2004 at 16:00–20:00 UT), the Cassini spacecraft was located outside the dust region where our analysis would be too complex (see section 2.2.2.1). It was also located inside the secondary electron current region identified in G12, i.e., in the L shell range of 7–10 and at Z values below $-1.2 R_S$ ($R_S = 60,268$ km Saturn radius). (X, Y, Z) is the Saturn-centered equatorial coordinate system, with Z pointing northward along Saturn's spin axis and X in the Saturn equatorial plane positive toward the Sun. The second period occurred during a high-inclination orbit on 17 and 18 May 2008, respectively, at 19:30–20:10 UT and 1:40–2:10 UT during the inbound and outbound legs of the orbit. The spacecraft was located in the same region (with L shell

ranges of 7.4–9.9 and 7–9.6, respectively) and well off the equator at $|Z|$ values above ~ 2.75 and $2.45 R_S$, respectively.

[9] The large data set used for the statistical study consists of all the time intervals of the LP (more than 250,000 time intervals) from 1 February 2005 to 30 July 2008. Several selections of the large data set (with various added criteria, e.g., on the electron temperature or $|Z|$ values) will be used through the paper to extract the most appropriate data inside this large data set.

[10] The time intervals considered in the paper will always be those of the LP. All CAPS data were linearly interpolated to these time intervals. The influence of the interpolation process (induced by the different time resolutions between the LP and CAPS data) will be discussed in section 2.3.1.2.

2.2. Langmuir Probe Data
2.2.1. The Currents Measured by the LP
[11] The LP is a titanium nitride (TiN)-coated conductive titanium sphere. A bias voltage (U_B) is actively applied to the LP with respect to the spacecraft in order to detect the electrons or ions, depending on the sign of the potential U relative to the plasma ($U = U_B + V_{float}$; V_{float} being the floating potential of the probe, considered uniform around the probe [*Nilsson*, 2009]). The bias voltage varies between –32 and +32 V in the magnetosphere. This allows the LP to detect the whole distribution of cold electrons or low velocity ions and to determine their characteristics. This does, however, not prevent the impact by energetic particles (e.g., hundreds of eV electrons) that cannot be repelled.

[12] The derivation of the cold plasma parameters (e.g., electron density n_e and temperature T_e) is performed through the fitting of the current-voltage (I-V) curve [*Fahleson et al.*, 1974] using the Orbital Motion Limited (OML) theory [*Mott-Smith and Langmuir*, 1926]. The usage of the OML theory is here justified since our study investigates the thin Saturnian magnetospheric plasma whose Debye length is much larger than the probe radius: e.g., the Debye length is typically above 2.5 m (compared with the LP radius of 0.025 m) at the equator near $L = 6$ for a density of 30 cm^{-3} and a temperature of 4 eV [*Persoon et al.*, 2009].

[13] The ion side current (I_-) measured for a negative potential (U) is given by

$$I_- = I_{ions} + I_{el} + I^* + I_{dust} + I_{ph} + I_{sec}^d + I_{sec}^* \tag{1}$$

where I_{ions} and I_{el} are the (thermal and ram) currents, respectively, due to the ambient cold ions and electrons, I_{dust} is the direct charged dust current to the probe, I^* the current due to the direct impact of energetic electrons and ions, I_{ph} the photoelectron current due to the photoionization of the probe surface, I_{sec}^d the current of secondary electrons induced by the impact of dust, and I_{sec}^* the current of secondary electrons induced by the impact of energetic particles.

[14] Only the ram/thermal ion and photoelectron currents are usually considered for negative probe potentials, since the cold electrons are repelled by the negative potential of the probe, the dust is located in specific regions near the equator, and the contribution by the energetic particles (both I^* and I_{sec}^*) is typically neglected. G12 showed, however, that this energetic contribution could be very significant at Saturn, in particular in the dipole L shell range of ~ 6–10 where the 250–450 eV are the most important. Our work

aims at modeling as precisely as possible the current due to the energetic electrons and then being able to remove it from the observations.

[15] The current for negative potentials I_- actually depends linearly on the bias potential at large negative U_B values, so that I_- is parametrized by a linear equation during the data analysis process:

$$I_- = m - bU_B \qquad (2)$$

where m and b are, respectively, the DC level (corrected for the spacecraft attitude) and slope of the fitted current-voltage curve on the ion side. These two parameters are the most important observables of the LP and then used to derive the plasma parameters. We will show later in our study that (and how) the energetic particles impact both the DC level m (through the added I_{ener} current identified by G12) and the slope b (through a contribution b_{ener}; see section 2.2.2).

[16] The m current has a random noise level of 0.1 nA (measured in laboratory; Wahlund, private communication). The derivation of the photoelectron current induces both a random noise level of 0.05 nA and a possible systematic error below 0.1 nA [Holmberg et al., 2012; Holmberg, private communication]. The systematic error may be induced by several issues which are today not taken into account, such as a partial shadowing of the probe surface from a boom or an antenna and partial ring eclipses.

2.2.2. Extracting the Energetic DC Level (I_{ener}) and Slope (b_{ener})

[17] As demonstrated by G12, the energetic 250–450 eV electrons impacting the probe generate secondary electrons and modify the current measured by the LP for negative potentials. This does not impact only the DC level m (through the I_{ener} current identified by these authors) but also the slope b of the current-voltage curve (through an added contribution b_{ener}). Understanding this influence implies first that we are able to extract both I_{ener} and b_{ener} from the measurements.

2.2.2.1. Extracting I_{ener}

[18] The current I_{ener} induced by the energetic particles impacting the probe—through the direct impact (I^*) and the secondary electrons produced (I^*_{sec})—may be extracted as follows from the LP measurements (see section 3 of G12 for the full development):

$$I_{ener} = m + bV_{float} - I_{i_0} - I_{ph} \qquad (3)$$

with I_{i_0} the "random ion current" defined by $I_{i_0} = I_{ions} + bU$ and given by the various contributions of each ith ion species [Fahleson et al., 1974]:

$$I_{i_0} = -\sum_i A_{LP} q_i n_i \sqrt{\frac{v_i^2}{16} + \frac{k_B T_i}{2\pi m_i}} \qquad (4)$$

with A_{LP} the surface of the probe, k_B the Boltzmann constant, and n_i, T_i, q_i, v_i, and m_i the density, temperature, charge state (essentially $+e$ at Saturn, with e the electron charge), drift speed (in the frame of the LP), and mass of the ith ion species. The ion parameters are not provided for each ion species by the LP: it can provide global (density weighted) values but cannot separate the contribution of each species.

[19] The usage of equation (3) to extract the current I_{ener} is based, beyond the analysis of the LP observations, on several assumptions:

[20] 1. The dust-induced currents I_{dust} and I^d_{sec} shall be negligible to derive equation (3); Wang et al. [2006] and Tsintikidis et al. [1994] showed that the dust is confined inside a layer of 1000–3000 km thickness around the equator; the influence of the dust currents will thus be removed if we focus on regions off the equator (e.g., $|Z| > 1 R_S$).

[21] 2. The photoelectron current I_{ph} shall be properly estimated; the values derived by Holmberg et al. [2012] were used in our analysis; moreover, all data occurring in eclipse for the LP (including the eclipses due to the spacecraft) were removed from the data set.

[22] 3. The cold ion thermal or ram current I_{i_0}, which is strong near the equator where the dominating water group ions are centrifugally confined [Sittler et al., 2008], must also be taken into account in principle; the first method is to choose time periods were the spacecraft is so far above the equator (e.g., $|Z| > 2 R_S$; see section 2.3.2 for more details) that one can neglect this current compared to the other currents; the second method is to calculate the current based on the knowledge of the various parameters included in I_{i_0} (in particular the ion parameters described in section 2.3.2).

[23] For the chosen case studies, all these stages were performed for extracting I_{ener}, with the I_{i_0} contribution calculated from the knowledge of the CAPS ion parameters described in section 2.3.2. However, as this procedure is complex, it cannot be applied to the large data set and a simpler method will be used, where I_{ener} is approximated by $m_{ion} = m - I_{ph}$. The contributions by $b \times V_{float}$ and I_{i_0} will indeed be neglected in equation (3) based on the following arguments. The contribution of $b \times V_{float}$ is negligible compared with m: b is of the order of 10^{-3}–10^{-2} nA/V and V_{float} is of the order of a few volts, whereas m is of the order of 0.5–1.5 nA (see Figure 5). Moreover, the contribution of the thermal ions via I_{i_0} may be neglected as soon as the data close to the equator are removed (see section 2.3.2).

2.2.2.2. Extracting b_{ener}

[24] The influence of the energetic particles is neglected in the Langmuir probe measurements discussed in the literature, and this is particularly true regarding the slope b of the current-voltage curve. As it will be discussed indeed in section 3, we found unexpected values of the b slope, precisely in the secondary electron current region where the current I_{ener} was identified by G12. We will show (see sections 3, 4, and 5) that the energetic electrons also impact the slope through a contribution b_{ener} defined by

$$b = b_{ions} + b_{ener} \qquad (5)$$

where b_{ions} is the classic contribution of the ambient ions to the slope b of the current-voltage curve, given by [Fahleson et al., 1974; Holmberg et al., 2012]:

$$b_{ions} = -\sum_i A_{LP} q_i n_i \sqrt{\frac{v_i^2}{16} + \frac{k_B T_i}{2\pi m_i}} \frac{e}{m_i v_i^2/2 + k_B T_i} \qquad (6)$$

[25] Extracting the contribution b_{ener} also implies the same assumptions as for the extraction of I_{ener} (see section 2.2.2.1). The original b value will, however, be used for the analysis of the large data set, since b is close to b_{ener} when we focus on the data where the spacecraft is off the equator ($|Z| > 2 R_S$) far from the dense plasma disk (see section 2.3.2).

2.3. The Cassini CAPS Electron and Ion Data
2.3.1. The Electron Data

[26] Three different types of CAPS ELS (ELectron Spectrometer) electron data were used in this paper and will be described below, corresponding to three different methods (detailed in sections 4 and 5 and compared in section 6) to reproduce the observed I_{ener} and b_{ener} contributions: the full electron distribution over all CAPS ELS channels, the average differential number fluxes (keV cm^2 sr s)$^{-1}$ over the 253–474 eV electrons only (which were identified by G12 as driving the current I_{ener}), and the electron moments (n_e, T_e).

[27] The first two data sets are identical to the data used in G12. The three types of data will be used for both the case studies and the large data set (defined in section 2.1), except the full distribution which could not be extracted for the large data set given the size of the files associated. Moreover, we used only the CAPS data from anode 5, which is the least affected by the spacecraft structures.
2.3.1.1. The Full CAPS ELS Distribution

[28] The full electron distribution is used for the case studies (SOI and high-inclination orbit). It consists of the differential number fluxes (keV cm^2 sr s)$^{-1}$ of all 63 energy channels from 0.53 eV/q (lower value of bin number 63) up to 28.3 keV/q (upper value of bin number 1). These data were corrected neither for noise (on the contrary to the other data sets; see below) nor for other artifacts such as the obscuration of parts of the spacecraft bus or the focusing of electrons in the nonuniform spacecraft potential. However, insofar as our study focuses on the secondary electron current region (i.e., outside the radiations belts), the noise which might affect our investigation essentially comes from the spacecraft radioisotope thermoelectric generators. This background noise level was estimated by *Arridge et al.* [2009] at 20–30 counts/s for anode 5 used in our paper [see *Arridge et al.*, 2009, Figure A2 in Appendix A]. During the case studies, the mean signal-to-noise ratio (ratio between the counts/s measured and the counts/s noise level) decreased from 240 to 3.1 with the energy (i.e., from bin number 63 to bin number 1), assuming a noise level value of 30 counts/s. In particular, the mean signal-to-noise ratio was 32–33 for 253–474 eV electrons. In addition, the data were averaged over 60 s time periods before the interpolation to the LP time intervals. The results discussed later for the case studies will thus not be affected by the noise sources.
2.3.1.2. The 253–474 eV Electrons

[29] The differential number fluxes discussed above were averaged during the case studies over channels 34 to 37 (energies between 253 and 474 eV) to obtain a mean flux value with a 1 min resolution. We remind that this energy range corresponds to the peak energy of the secondary electron yield function for the surface of the LP. This explains why G12 observed a strong correlation between the detected current I_{ener} and these energetic electrons.

[30] We also used the same energy range for the large data set from 2005 to 2008. The differential number fluxes were, however, averaged over 10 min time intervals given the size of the file associated: 207,542 time intervals, including the whole orbits and not only the crossings of the secondary electron current region. During this large period, we removed all the time intervals where the signal-to-noise ratio was below 1 (for a noise level of 30 counts/s), which concerned about 3.5% of the total data set.

[31] The CAPS electron data were averaged—over 1 min for the case studies or 10 min time intervals for the large data set—before they were interpolated at the LP time intervals. The influence of this procedure was analyzed for the mean 253–474 eV electron fluxes during the case studies. After the interpolation at the LP time intervals, we calculated the relative difference between the initially 1 min averaged fluxes and alternative data sets, such as the 15 or 30 s averaged fluxes or the 15 s median fluxes. The resulting relative difference after the interpolation process is of the order of 3.4–6.4% only. As a consequence, the difference between the initial time intervals of the CAPS and LP experiments, as well as the choice of the averaging process before the interpolation, will only very slightly impact our results.
2.3.1.3. The Electron Moments

[32] The third type of CAPS data used in this study is the 3D electron moments (n_e, T_e) derived by *Lewis et al.* [2008]. We first selected the data between 5 June 2004 and the end of 2008 (more than 4 million of time intervals with a time resolution of 32 s). The moments were then interpolated to the LP time intervals, both for the case studies and the statistical analysis from 2005 to 2008.

[33] The moments are not to be trusted for negative values of the spacecraft potential, also given by *Lewis et al.* [2008]. More precisely, since the lowest energy detected by CAPS is 0.6 eV, a threshold at 0.6 V or—to avoid checking for the number of counts measured—at 1 V is appropriate to avoid the data which cannot be trusted (G. Lewis, private communication). A threshold at 1 V was used for the large data set but not for the case studies, where two thirds of the time intervals should be removed. The spacecraft potential is indeed between 0.5 and 1 V during two thirds of the case studies time intervals. However, the electron moments are still correct during the time intervals, since the potential is still positive and the number of counts/second is large (always above $\sim$ 270) during both the SOI and high-inclination periods.
2.3.2. The Ion Data

[34] As explained in section 2.2.2, the extraction of the energetic contributions I_{ener} and b_{ener} to the respective DC level and slope of the current-voltage curve needs the estimation of the thermal ion parameters (see equations (4) and (6)).

[35] We used, for the analysis of the case studies, the ion data published by *Sittler et al.* [2006] for the SOI period and those published by *Thomsen et al.* [2010] for the high-inclination orbit (M. Thomsen, private communication). The ion data were then interpolated to the LP time intervals. The *Sittler et al.* [2006] results include both water group ions ($m_W = 17$ amu) and protons ($m_H = 1$ amu), whereas *Thomsen et al.* [2010] also include the contribution of H_2^+ ions ($m_i/q_i = 2$). Both works provide the following parameters for each ion species: n_i, T_i, and v_i. v_i was determined from the three components of the velocity vector (radial, azimuthal, and vertical) except for the SOI period where *Sittler et al.* [2006] assumed a zero vertical velocity.

[36] The thermal ions contribute to the DC level (m) and slope (b) of the current-voltage curve through the respective I_{i0} and b_{ions} parameters. These contribute, respectively, on average to $\sim$ 5% and $\sim$ 30% of the total m and b values measured during the case studies. The influence of the ions is thus negligible regarding the DC level but not really for
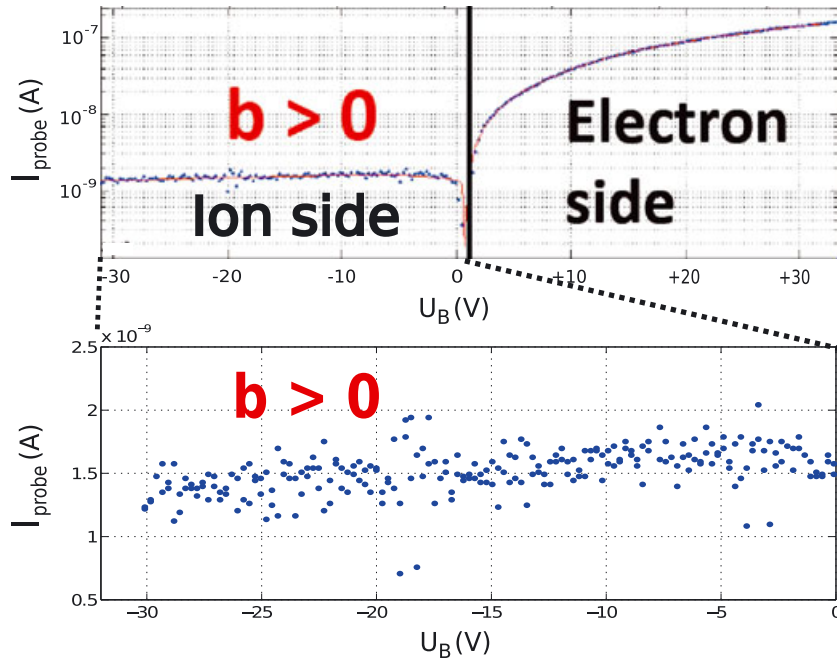
Figure 1. Example of sweep for the LP (18 December 2007 at 21:13 UT), with the current measured as a function of the bias voltage U_B applied to the probe. (top) The whole sweep and (bottom) the negative potential part. At negative potentials, the probe attracts essentially ions but shows an unusual positive slope b.

the slope, in particular during SOI where the spacecraft was located closer to the equator (with $|Z| \geq 1.2\,R_S$) than during the high-inclination periods (where $|Z| \geq 2.45\,R_S$).

[37] We introduced the influence of the thermal ions in the analysis of the case studies but not for the large data set given the complexity of the ion parameters derivation. This will not impact our results regarding the DC level, and the impact will still be small for the slope by selecting periods where the spacecraft was above $2\,R_S$ off the equator.

3. Unusual Positive Values for the Slope of the Current-Voltage Curve

[38] In this section, we will show and interpret the observations of unusual positive values of the b slope of the current-voltage curve of the LP, observed mostly in the secondary electron current region.

3.1. The Langmuir Probe Observations

[39] The active application to the LP of a variable bias potential U_B between –32 and +32 V (called a "sweep") leads to the plotting of the current-voltage curve. For negative potentials, this curve may be fitted by a linear function (see equation (2)) whose slope b is given by

$$b = -\frac{I(U_B = -5\,\text{V}) - I(U_B = -32\,\text{V})}{-5 + 32} \qquad (7)$$

[40] Since the currents for incoming ions are defined as negative (respectively, positive for incoming electrons), more negative U_B values lead to more negative currents due to more attracted ions, which in the end gives negative values for b. This is also expected from theory, since we classically have $b = b_{\text{ions}}$ where b_{ions} is negative according to equation (6). The current-voltage curve thus usually shows a

negative value of the slope b, as observed in any ionosphere (see examples of such curves by *Wahlund et al.* [2005a] or *Ågren et al.* [2007] at Titan).

[41] However, as can be seen in Figure 1, we can find LP sweeps where b is actually positive. This figure shows the current-voltage curve measured on 18 December 2007 at 21:13 UT. Figure 1 (top, left) corresponds to negative potentials U, where the ions are attracted. The slope b is thus clearly positive.

[42] Figure 2 shows the occurrence of such events as a function of the L shell, for the large data set with all LP data from 1 February 2005 to 30 July 2008. The figure also gives the radial profile of the normalized electron differential number fluxes (for the energy range 253–474 eV) for the same period. The observed profiles are very similar to those in G12 (Figure 4) which compared the estimated I_{ener} and the same electron number fluxes. The presence of positive values of b is indeed very common (up to $\sim 83\%$ of the data) in the secondary electron current region off the equator, where the energetic electrons fluxes are high. Such events may even still be seen in the outer magnetosphere, with a smaller occurrence though. Furthermore, mapping the b parameter as a function of both L shell and local time (not shown) gives also a similar distribution to the one of I_{ener} in Figure 1 of G12. Such a mapping indeed reveals values larger on the nightside than on the dayside, which is related to the asymmetries observed for the hundreds eV electrons by *DeJong et al.* [2011].

[43] One can thus conclude that the energetic electrons impact not only the DC level of the current-voltage curve at negative potentials (through the contribution I_{ener}) but also the slope b of this curve (through a contribution b_{ener} defined by $b_{\text{ener}} = b - b_{\text{ions}}$).
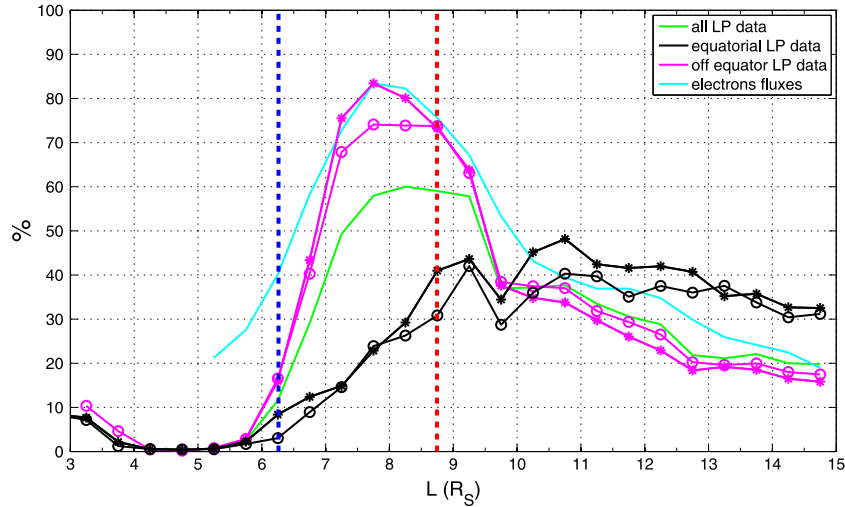
Figure 2. Occurrence (in percent) of positive values of the slope b as a function of L shell, for all LP data from 1 February 2005 to 30 July 2008. The red, black, and magenta lines represent, respectively, the occurrences for all time intervals, those with Cassini near the equator, and those off the equator. Two different limits were used for the definition of "equatorial data" and "off equator data": $|Z| > 1 R_S$ (o symbol) and $|Z| > 2 R_S$ (* symbol). The cyan line gives the normalized CAPS electron differential number fluxes $(\text{keV cm}^2 \text{ sr s})^{-1}$ for the energy range 253–474 eV. The thick blue and red vertical dashed lines show the L shell values of Dione and Rhea.

3.2. Interpretation

3.2.1. The Balance Between the Incident and Secondary Electrons

[44] The observation of positive slopes of spacecraft current-voltage curves has already been discussed in the past, in particular in the context of the "triple roots" situations. The charging of a spacecraft indeed obeys the current balance equation with all incoming and outgoing currents. This equation is satisfied for a specific potential (floating potential) that is a root for the equation. *Whipple* [1965] and *Prokopenko and Laframboise* [1980] showed that in some cases, the presence of secondary electrons may induce reversals of the current-voltage curve. It may also lead to several roots, with the spacecraft thus jumping from a floating potential to another.

[45] Our positive slope observations can be explained as follows. On the negative side (negative potentials) of the current-voltage curve, the current due to the collected ions (I_{ions}; defined negative) increases in absolute value at large negative potentials, since the surface attracts more and more ions. This leads to a classical negative slope b as defined by equations (6) and (7). In the same time, the incident electrons are more and more repelled and I_{el} (defined positive) thus decreases at large negative potentials. The secondary electrons current induced by the impact of the incident electrons (defined negative) also decreases in absolute value since there are less incident electrons. Consequently, if there are more secondary than incident electrons (i.e., if the secondary electron yield is greater than 1), then the total (incident + secondary) electron current is negative and has a positive slope. In the end, if the ion current is smaller than the total (incident + secondary) electron current, the slope b observed will be positive.

[46] Figure 3 shows a zoom of the current-voltage curve example previously shown in Figure 1, where we added

the individual current contributions. The ion contribution I_{ions} (not shown) may be neglected since the spacecraft is far off the equator ($Z \sim 2.6 R_S$). The total current due to the energetic electrons—incident + secondary electrons—was modeled with the theoretical moments approach described later in detail (see section 5 and equation (11) in particular). Adding this contribution to the photoelectrons current I_{ph} allows to reproduce very closely the measurements.

3.2.2. Identification of the Critical/Anticritical Temperatures

[47] The key factor leading to positive slopes is the presence of more secondary than incident electrons. The ratio between secondary and incident electrons as a function of the energy is given for any material by the secondary electron emission yield (SEEY). This yield is known to peak (with a yield above one) at incident electron energies near 200–1000 eV for metal layers [*Hastings and Garrett*, 1996]. The peak energy for the Cassini LP was determined by G12 close to 350 eV, in agreement with laboratory measurements of TiN surfaces by *Walters and Ma* [2001] or *Lorkiewicz et al.* [2007]. The exact form and the maximum yield value are, however, essentially unknown and will be discussed further in sections 5.1.2.1 and 5.3.

[48] *Laframboise et al.* [1982] and *Lai et al.* [1983] were the first to introduce the concept of "threshold temperature" or "critical temperature" for the spacecraft charging. The SEEY curve indeed implies the existence of an electron temperature of the ambient plasma below which there will be less incident than secondary (and backscattered) electrons. A surface material thus cannot be charged negatively in this plasma environment. Above the critical temperature T_* specific for each surface composition, one may observe high-voltage charging events such as the kV spacecraft potentials first observed in the Earth plasmasheet by geosynchronous satellites [*DeForest*, 1972].
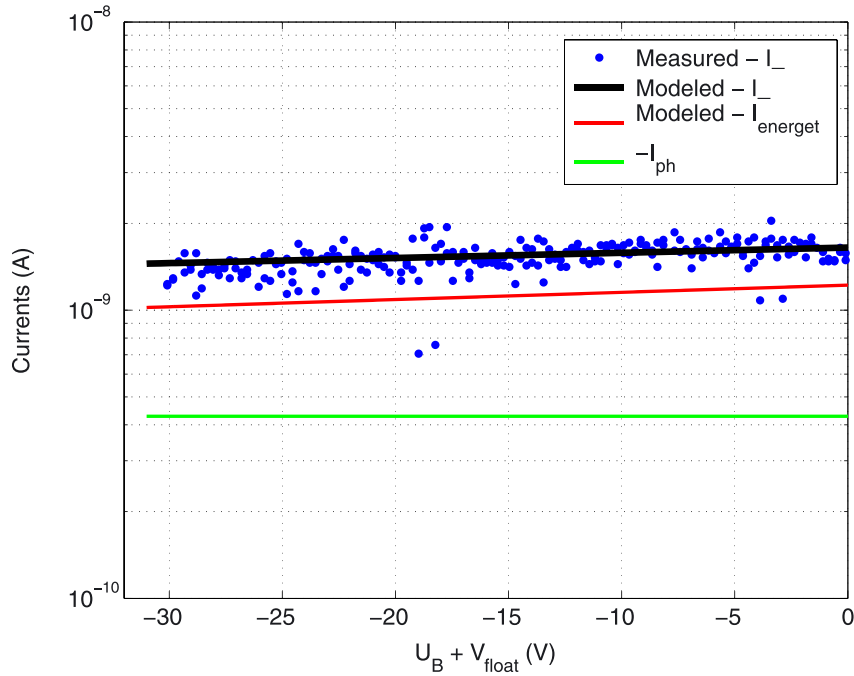
Figure 3. Negative potential side of the Figure 1 current-voltage curve obtained on 18 December 2007 at 21:13 UT. The total measured I_- current (blue dots) is compared with the modeled I_- current (black line) derived from the addition of the photoelectron current (I_{ph}, green line) and the current due to the energetic electrons ($I_{energet}$, defined by equation (11) where $n_e = 1.28 \, cm^{-3}$, $T_e = 173.5$ eV, $V_{float} = 0.62$ V, and $\delta_{e_{max}} = 1.22$; see section 5 for more details about the theoretical moments approach).

[49] Similarly, *Lai and Tautz* [2008] recently predicted the existence of an anticritical temperature T_A, which is the low-energy symmetric value for the critical temperature T_*. The SEEY curve indeed peaks at a certain energy, inducing two temperatures where the number of incident and secondary (+ backscattered) electrons are identical. Above T_A and below T_*, the number of secondary (and backscattered) electrons will be larger than the number of incident electrons. A metal surface embedded in a Maxwellian plasma whose temperature is in the range $[T_A; T_*]$ thus cannot be negatively charged. If some evidence was already found for the existence of critical temperatures in experimental data [e.g., *Olsen*, 1983; *Lai and Tautz*, 2006], no evidence was found (as far as we know) for the existence of the anticritical temperatures.

[50] Figure 4 shows such evidence for the Cassini LP. The slope b measured is shown as a function of the electron temperature of the ambient plasma measured by CAPS. The data set corresponds to the 2005–2008 LP measurements off the equator ($|Z| > 2 R_S$) and inside the secondary electron current region ($6.4 < L < 9.4$), which implies that the b slope is essentially the b_{ener} contribution due to energetic electrons. Two profiles are shown: corrected or not for the measurements with low spacecraft potentials (< 1 V; see section 2.3.1.3). We added the profile not corrected for comparison: the statistics is better ($\sim 40\%$ more events) and except for the rare low electron temperature (i.e., few eV) events in our data set, the electron temperature measured should not be affected by including the low potentials.
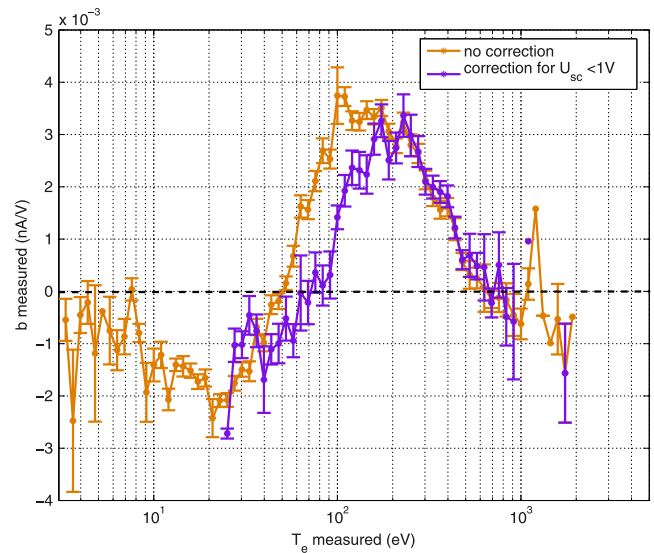

Figure 4. Slope b (i.e., approximate b_{ener} given the data selection) of the LP current-voltage curve as a function of the incident electron temperature T_e measured by CAPS. The data set corresponds to all data with $6.4 < L < 9.4$ and $|Z| > 2 R_S$ between 1 February 2005 and 30 July 2008. The CAPS data do either take into account (orange) or not (violet) the intervals with low spacecraft potential values (i.e., $U_{sc} < 1$ V). The standard deviations are also shown for each profile.

[51] As will be developed in detail in section 5.1.3.1, b_{ener} may be considered as proportional to

$$\alpha = \int_0^\infty E f_{ie}(E)(1 - \delta_e(E) - \eta_e(E))\mathrm{d}E \qquad (8)$$

with $f_{ie}(E)$ the incident electron distribution function at energy E, $\delta_e(E)$ the SEEY yield value, and $\eta_e(E)$ the backscattering coefficient (see section 5.1.2 for further details). This quantity actually corresponds to the balance between the incident electrons and the secondary/backscattered electrons. Thus, the temperatures T_A and T_*, where there is an equilibrium between the incoming and the outgoing electrons (i.e., when $\alpha = 0$), also correspond to the temperatures where b_{ener} is null in the figure.

[52] Consequently, Figure 4 suggests that the critical and anticritical temperatures for the Cassini LP surface are, respectively, at ~ 600–$800\,\mathrm{eV}$ and ~ 50–$60\,\mathrm{eV}$. These values are in agreement with the broad range of values proposed by *Lai and Tautz* [2008] for a set of surface materials. As shown in section 5.1.3.2, the energetic contribution I_{ener} to the DC level of the current-voltage curve may also be considered as proportional to the quantity α and shows a similar curve (not shown) as a function of the electron temperature. The DC level is, however, less convenient to derive values for T_A and T_*.

[53] One can also infer from the $b_{ener} = f(T_e)$ profile that the influence of the energetic electrons, though present for any incident electron temperature, will be maximum in the range $[T_A; T_*]$, i.e., where the SEEY is maximum. In the sections below, an additional criterion—beyond the criteria for L and Z values—on the incident electron temperature (e.g., $100 < T_e < 500\,\mathrm{eV}$) will be used to select appropriate time intervals for the modeling of the energetic electrons influence.

4. A First Approach to Estimate I_{ener} and b_{ener}: The Statistical Correlation With the 250–450 eV Electrons

[54] In this section, we will investigate a first method to reproduce the observed values of I_{ener}/b_{ener} based on statistical fits with the differential number flux of 253–474 eV electrons. We will deduce from this analysis to what extent the slope b may be used to identify the regions where the energetic electrons have a strong impact.

4.1. A Statistical Analysis

[55] We showed in G12 and in section 3 above that the I_{ener} and b_{ener} observations are correlated with the 253–474 eV electrons, i.e., the peak energy of the SEEY function for the LP surface. We thus investigated this correlation further.

[56] Figure 5 shows these correlations with the m_{ion} and b values measured from 1 February 2005 to 30 July 2008, with two different selections among this large data set. Selection 1 corresponds to the periods when the spacecraft was located off the equator at $|Z| > 2\,R_S$ and inside the secondary electron current region in the L range 6.4–9.4 R_S (without any criterion on the electron temperature). Selection 2 is a subselection of selection 1, with the CAPS-derived electron temperatures between 100 and 500 eV. The criteria used in these selections allow us to consider m_{ion} and b as close to the energetic DC level and slope I_{ener} and b_{ener} since the con-

tribution of thermal ions should be small. Selection 2 focuses on the electron temperature range identified in section 3.2 as the range where the influence of the energetic electrons is the strongest.

[57] The best fit third-order polynomial functions are superimposed in each panel, with the following equations (x being the electron flux) and associated Pearson's correlation coefficients r [*Press et al.*, 2007]:

[58] 1. Figure 5a: $m_{ion} = -3 \times 10^{-24}x^3 + 9 \times 10^{-16}x^2 - 7 \times 10^{-8}x + 0.0336$; $r = 0.793$.

[59] 2. Figure 5b: $b = 2 \times 10^{-25}x^3 - 2 \times 10^{-17}x^2 + 7 \times 10^{-10}x - 0.0024$; $r = 0.578$.

[60] 3. Figure 5c: $m_{ion} = 3 \times 10^{-23}x^3 - 1 \times 10^{-15}x^2 - 4 \times 10^{-8}x - 0.0567$; $r = 0.802$.

[61] 4. Figure 5d: $b = -2 \times 10^{-26}x^3 + 6 \times 10^{-20}x^2 + 3 \times 10^{-10}x - 0.0008$; $r = 0.668$.

[62] These results show a dispersion of the data, but the best fits functions provide a good estimation of m_{ion} and b (i.e., I_{ener} and b_{ener} given the selections criteria). The estimation is better for the DC level than for the slope with respective correlation factors of ~ 0.8 and ~ 0.6–0.65. Selecting the intervals with electron temperatures between 100 and 500 eV also ameliorates the correlation by about 0.1. This confirms again that these electrons are those which induce the largest energetic contributions I_{ener} and b_{ener}.

[63] The plots also allow to see a threshold effect, i.e., the existence of a minimum flux value for the incident electrons to influence the two parameters and start the increase observed. This threshold is approximately between 1 and 3×10^6 (keV cm^2 sr s)$^{-1}$.

[64] The selections used above correspond to the L range 6.4–9.4 R_S, where large 253–474 eV electron differential number fluxes are often observed, but such energetic electrons are also present further in the magnetosphere. A statistical analysis (for the same data set) shows a decreasing occurrence of such large fluxes with L, but more than a third of the data show 253–474 eV fluxes above 1×10^6 (keV cm^2 sr s)$^{-1}$ at $L = 16\,R_S$. The data were selected in this paper in order to reproduce accurately the influence of energetic electrons, but such an influence (though reduced) does exist in a large part of the Saturnian magnetosphere.

[65] One should add that the flux threshold observed corresponds to the minimum flux to detect the influence of the energetic electrons given the data set considered, i.e., so that the energetic current is not masked by the ion current. Our data set selection allowed to remove most of the ion current contribution, so that the threshold values identified are very close to the "real" threshold that would be observed in the total absence of ion contribution. However, if we changed our data set selection criteria to include data closer to the equator, allowing the presence of larger ion currents, the flux threshold would probably be observed at higher values.

4.2. The Slope b as a Criterion to Identify the Regions Influenced by the Energetic Electrons

[66] The influence of the energetic electrons on the current-voltage curve of the LP may be considered as a parasite for the thermal plasma measurements. It would be important to be able to identify the data which are parasited by such a contribution. Is the observation of positive values for the slope b a possible criterion?
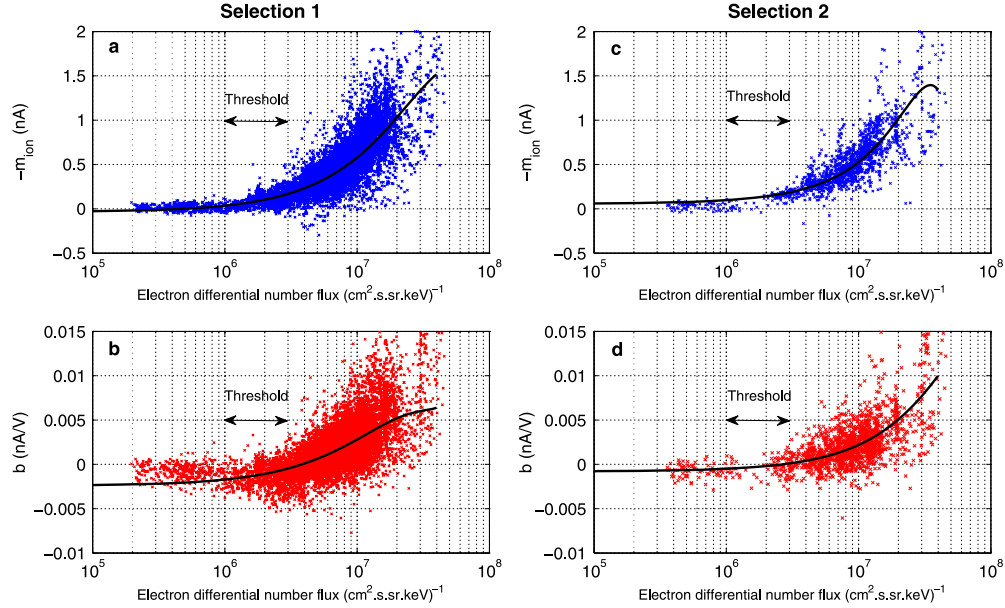
Figure 5. (a, c) $-m_{ion}$ (i.e., approximate $-I_{ener}$) and (b, d) b slope (i.e., approximate b_{ener}) values measured by the LP as a function of the CAPS mean differential number flux of the 253–474 eV electrons. Two data sets are used here, corresponding to two selections of the data from 1 February 2005 to 30 July 2008. Selection 1 (in Figures 5a and 5b) corresponds to the data when the spacecraft was located off the equator at $|Z| > 2 R_S$ and inside the secondary electron current region in the L range 6.4–9.4 R_S. Selection 2 (in Figures 5c and 5d) is a subselection of selection 1, with the CAPS-derived electron temperatures between 100 and 500 eV. The solid black lines show the best fit third-order polynomial functions for each panel (see text for the equations used). The double arrows show the threshold flux values ($[1 - 3] \times 10^6$ (keV cm² sr s)$^{-1}$) above which the incident energetic electrons influence the $-m_{ion}$ and b parameters.

[67] Figure 6 shows the occurrence, for the large data set, of positive b values as a function of the minimum 253–474 eV electron differential number flux considered. The occurrence strongly increases when only large fluxes are selected, and goes beyond 50% above fluxes of $\sim 3 \times 10^6$ (keV sr s)$^{-1}$ up to values above 90%. Most of the slope values are thus positive when the electron flux is beyond the flux threshold which induces the appearance of the energetic contributions I_{ener} and b_{ener} (threshold identified in the previous section). However, there also exists positive values of b even for low electron fluxes (minimum 20%). As a consequence, the only observation of positive slope values cannot be used as a criterion to identify the regions significantly influenced by the energetic electrons.

[68] Figure 7 shows the occurrence of electron fluxes above the flux threshold (three different values are considered) as a function of the minimum b value. If we assume that the influence of the energetic electrons appears with fluxes larger than the threshold value, then large values of the slope may be a good criterion to identify such events. For example, $\sim 80\%$ of the data show electron fluxes above a threshold at 1 (respectively, 3) $\times 10^6$ (keV cm² sr s)$^{-1}$ when b is larger than ~ 2.1 (respectively, 2.8) $\times 10^{-3}$ nA/V.

[69] The observation of large positive slope values may probably be used as a simple criterion during the LP analysis process to identify the regions where the energetic electrons have a significant influence. The limit b value to be used may be chosen depending on the probability wanted. The limit value may, however, be different in other environments (such as other magnetospheres than Saturn), whereas the cri-

terion over the electron temperature depends only on the probe surface composition.

4.3. Application to the Case Studies

[70] The statistical analysis developed in section 4.1 was based on the large data set in order to obtain the best fit functions. Figure 8 shows the application of these fits to
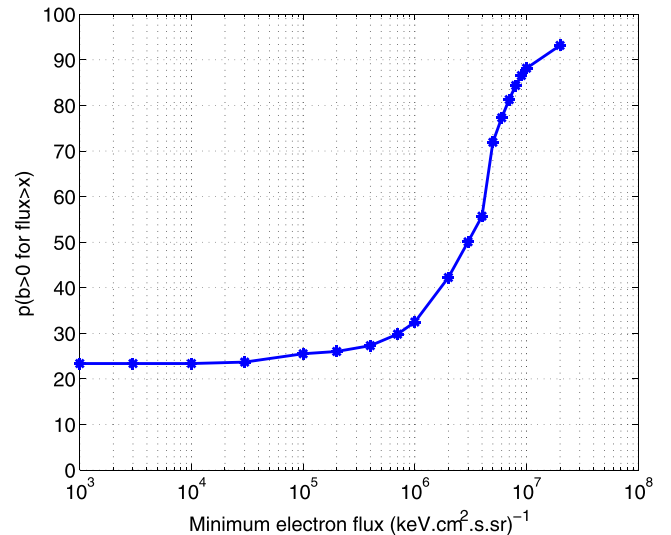

Figure 6. Probability of positive b values as a function the minimum electron differential number flux value considered for the 253–474 eV incident electrons.
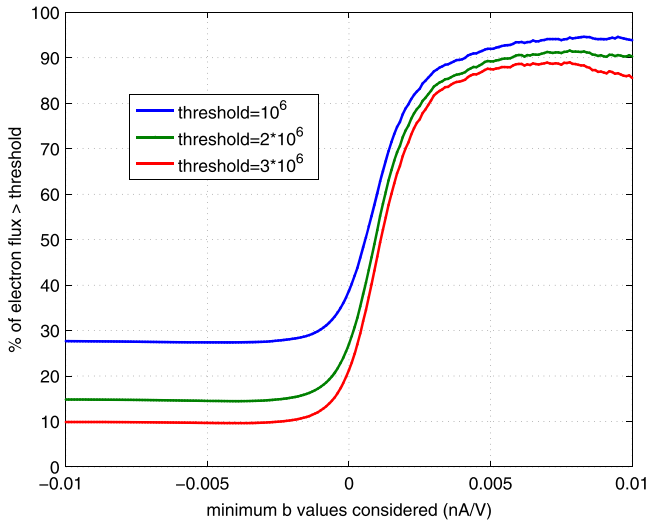
Figure 7. Probability of observing (253–474 eV) incident electron differential number fluxes above a certain threshold, as a function of the b value considered. Three different thresholds were considered ($1/2/3 \times 10^6$ (keV cm^2 sr s)$^{-1}$), leading to three probability curves.

the case studies, with a comparison between the observed and estimated values of the energetic DC level and slope of the current-voltage curve. One can derive the same conclusions as from the large data set analysis, i.e., selections 1 and 2 functions give similar good results, and I_{ener} is better reproduced than b_{ener}.

[71] The less good correlation for the slope is probably related to the noisy dynamics of the observed b value. The

slope of the current-voltage is indeed small in absolute value in such low-density plasma environments, which probably leads to a noisy profile. The different time intervals between the CAPS and LP data may also be an explanation for the less good correlation: the interpolation process may hide the high dynamics of the electron flux.

[72] We refer the reader to section 6 for a comparative discussion on the precision of the various methods to reproduce the influence of the energetic electrons. The method using the 253–474 eV electron flux gives a good estimation of the I_{ener} and b_{ener} contributions. It is, however, only an empirical approach, with fit functions that cannot be applied directly to other plasma environments and that depend on the data set selection criteria used. As a consequence, one needs a more theoretical approach to understand further this influence.

5. A Second Approach: The Theoretical Influence of the Energetic Electrons

[73] In this section, we will use a theoretical approach to model the influence of the energetic electrons (incident, secondary, and backscattered), in order to reproduce the observed I_{ener} and b_{ener} contributions. We will first derive the appropriate equations (section 5.1) before we compare with the observations (section 5.2) and infer the most appropriate maximum yield value $\delta_{e_{\max}}$ (section 5.3) for the LP.

5.1. The Derivation of the Equations

[74] We will first determine the equation for the total current of incident/secondary/backscattered electrons at any bias voltage U_B (section 5.1.1) before we detail the input parameters needed (section 5.1.2) and infer the equations for I_{ener} and b_{ener} (section 5.1.3).
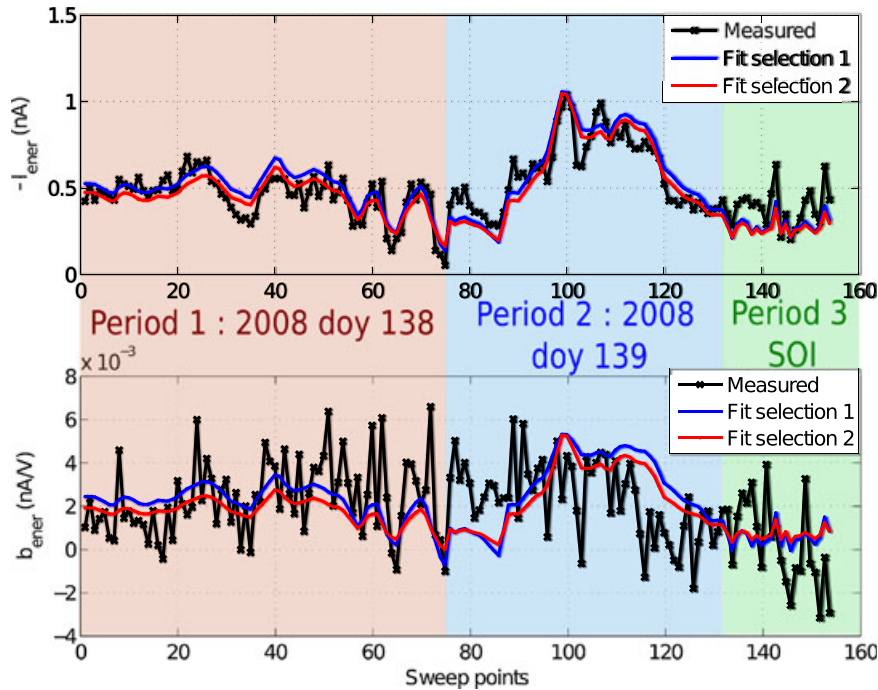

Figure 8. (top) $-I_{\text{ener}}$ and (bottom) b_{ener} measured (black) and estimated with the flux method fit functions during the case studies (inbound and outbound legs of the high-inclination orbit, SOI). Two fit functions were used for each parameter, corresponding to the data from selections 1 (blue) and 2 (red).

5.1.1. The Current Due to the Energetic Electrons

[75] Modeling the exact current due to the energetic electrons is a very difficult task, due to the complex influence of several parameters: the influence of the floating potential, of the sheath effects from the LP (due to a finite ratio between the sheath radius and the probe radius), the exact angular and energy distribution of the secondaries, etc. Consequently, several approximations are considered in the literature to derive such equations, leading to several methods.

[76] *Hastings and Garrett* [1996] proposed equations for the currents collected by a spacecraft for negative potentials. Assuming a Maxwellian distribution with a temperature T_{se} for the secondaries, their approach leads to the following total current for incident and secondary electrons:

$$I_{Hast} = -\frac{2\pi e}{m_e^2} A_{LP} \int_0^\infty f_{ie}(E) \int_0^\pi \sin(\theta) \qquad (9)$$
$$* (\delta_e(E, \theta + \pi/2)k_B T_{se} - E/2) \mathrm{d}\theta \, \mathrm{d}E$$

with f_{ie} the incident electron distribution function, θ the angle from the surface normal, and $\delta_e(E, \theta + \pi/2)$ the SEEY energy and angular function.

[77] The *Hastings and Garrett* [1996] approach does take explicitly into account the secondary electron distribution function and the angular dependence of the SEEY but not the (repelling) effect of the surface potential on the incident electrons or sheath effects. However, several limitations prevent the use of this approach. First, the equation above was corrected for several errors existing in *Hastings and Garrett* [1996] (confirmed by D. Hastings, private communication): missing E and factor 2 in their equation 5.7, $\pi/2$ missing in equation 5.6. But beyond these errors, the quantity $\delta_e(E, \theta + \pi/2)k_B T_{se} - E/2$ in equation (9) will always be negative for energetic plasma environments (e.g., $T_e > 10$ eV). This equation thus corresponds to a negligible contribution of the secondaries in the total current collected. As a consequence, the *Hastings and Garrett* [1996] approach cannot account for our observations.

[78] We chose as a first step the approach used by *Lai and Tautz* [2008], who proposed the following form for the total (incident/secondary/backscattered) electron current (for $U < 0$):

$$I_{Lai} \sim \int_0^\infty E f_{ie}(E) (1 - \delta_e(E) - \eta_e(E)) \mathrm{d}E * e^{\frac{eU}{k_B T_e}} \qquad (10)$$

[79] This approach uses a simplified expression for the influence of the surface potential (through the Boltzmann term $e^{\frac{eU}{k_B T_e}}$). Considering a corrected energy $E - eU$ instead of E for the secondary electrons would only slightly (by a few percent at maximum) change the results given the large electrons temperatures (hundreds of eV) and small potential values (a few volts). This approach provides a convenient analytical way to calculate the total current due to the energetic electrons. A normalization factor is, however, missing in equation (10) to derive the real current. Adding the normalization factor (by comparison with the expressions for spherical probes in *Mott-Smith and Langmuir* [1926]) leads

to the final expression for the total current $I_{energet}$ due to the energetic electrons:

$$I_{energet} = \frac{2\pi e}{m_e^2} A_{LP} \int_0^\infty E f_{ie}(E) (1 - \delta_e(E) - \eta_e(E)) \mathrm{d}E \qquad (11)$$
$$* e^{\frac{eU}{k_B T_e}}$$

[80] This total current $I_{energet}$ then impacts both the DC level and slope of the LP current-voltage curve through the respective contributions I_{ener} and b_{ener}, whose expressions will be derived later.

5.1.2. The Choice of the Input Parameters

[81] The calculation of the current due to the energetic electrons $I_{energet}$ needs the knowledge of the incident electron distribution function $f_{ie}(E)$ determined from the CAPS data (see later in section 5.2), but it also needs the knowledge of both the secondary electron emission yield function ($\delta_e(E)$; see section 5.1.2.1) and the backscattering coefficient ($\eta_e(E)$; see section 5.1.2.2).

5.1.2.1. The Secondary Electron Emission Yield Function

[82] Several functional forms of the SEEY as a function the incident electron energy were used in our study:

[83] 1. *Sternglass* [1957]: $\delta_e(E) = 7.4\delta_{e_{max}} \frac{E}{E_M} e^{-2\sqrt{\frac{E}{E_M}}}$.

[84] 2. *Lin and Joy* [2005]: $\delta_e(E) = 1.28\delta_{e_{max}} \frac{E}{E_M}^{-0.67} \left(1 - e^{-1.614\frac{E}{E_M}^{1.67}}\right)$.

[85] 3. *Sanders and Inouye* [1978]: $\delta_e(E) = c\left(e^{\frac{-E}{a}} - e^{\frac{-E}{b}}\right)$ with $a = 4.3E_M$, $b = 0.367E_M$ and $c = 1.37\delta_{e_{max}}$. with $\delta_{e_{max}}$ (maximum yield value) and E_M (peak energy) being free parameters to be determined for the LP surface composition. The $\delta_{e_{max}}$ value will be chosen arbitrarily at first in section 5.2. We will then propose a method to determine its best value and compare with laboratory measurements in section 5.3. The peak energy E_M is chosen at ~ 350 eV based on G12.

[86] Figure 9 shows a comparison between the three proposed yield functions, assuming an arbitrary value of $\delta_{e_{max}} = 2$. The yield by *Lin and Joy* [2005] is the largest at high energies and the smallest at low energies, whereas the function by *Sternglass* [1957] is the largest at low energies and close to *Sanders and Inouye* [1978] at high energies. The influence of the choice for the yield function is not significant as will be shown in section 5.2. A unique reference will be used, *Sanders and Inouye* [1978], since this yield curve is in between the two other references and its use is convenient for analytical integrations.

5.1.2.2. The Electron Backscattering Coefficient

[87] The backscattering electrons are mostly significant at low incident energies (few eV). A backscattering coefficient may be, however, included for detailed calculations. This coefficient depends on the exact surface composition, the incident electron energy, or the incidence angle of these electrons. Monte Carlo simulations (M. Belhadj, French Aerospace Laboratory, private communication) for TiN surfaces give $\eta_e(E) \approx 0.2$–0.4. We thus choose as a first step a constant backscattering coefficient at 0.3.

[88] Moreover, the secondary and backscattered electrons shall be considered together ($\eta_e + \delta_e$ in the equations). Insofar as the choice of $\delta_{e_{max}}$ is for the moment arbitrary in our study,
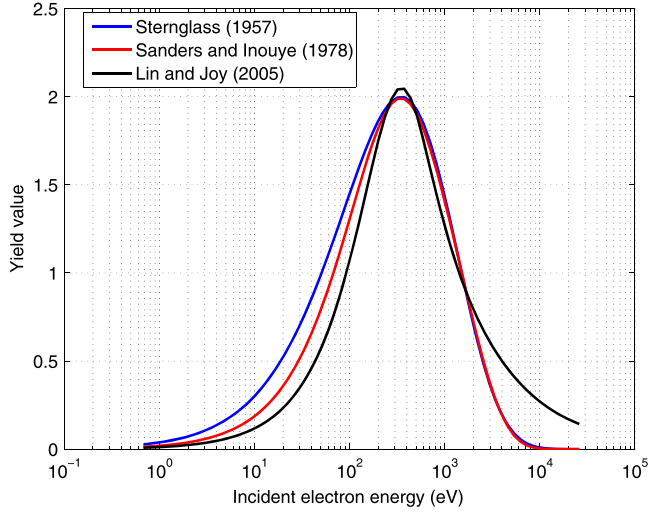
Figure 9. Comparison between three different secondary electron emission yield functions as a function of the energy of the incident electrons. The peak energy E_M is defined at 350 eV based on *Garnier et al.* [2012b], and an arbitrary value of 2 was chosen for the maximum yield $\delta_{e_{\max}}$.

the precise value of the constant $\eta_e(E)$ value has no significant influence: a slight change in $\eta_e(E)$ corresponds directly to a slightly different value for $\delta_{e_{\max}}$.

5.1.3. The Equations for the Energetic Electrons Contributions b_{ener} and I_{ener}

5.1.3.1. The b_{ener} Contribution

[89] The b slope of the current-voltage curve is defined by equation (7). Consequently, the b_{ener} contribution due to the energetic electrons is similarly given by

$$b_{\mathrm{ener}} = -\frac{I_{\mathrm{energet}}(U_{\mathrm{B}} = -5\,\mathrm{V}) - I_{\mathrm{energet}}(U_{\mathrm{B}} = -32\,\mathrm{V})}{-5 + 32} \quad (12)$$

Combining with equation (11) for I_{energet} leads to

$$b_{\mathrm{ener}} = -\frac{2\pi e}{m_e^2} A_{\mathrm{LP}}\left(\int_0^\infty E f_{\mathrm{ie}}(E)\left(1 - \delta_e(E) - \eta_e(E)\right)\mathrm{d}E\right)$$
$$* \frac{e^{\frac{e(V_{\mathrm{float}}-5)}{k_{\mathrm{B}}T_e}} - e^{\frac{e(V_{\mathrm{float}}-32)}{k_{\mathrm{B}}T_e}}}{32 - 5} \quad (13)$$

which can be written as

$$b_{\mathrm{ener}} = -\frac{I_0 A}{27} \quad (14)$$

with

$$I_0 = \frac{2\pi e}{m_e^2} A_{\mathrm{LP}}\left(\int_0^\infty E f_{\mathrm{ie}}(E)(1 - \delta_e(E) - \eta_e(E))\mathrm{d}E\right) \quad (15)$$

and (sinh hyperbolic sinus function)

$$A = e^{\frac{e(V_{\mathrm{float}}-5)}{k_{\mathrm{B}}T_e}} - e^{\frac{e(V_{\mathrm{float}}-32)}{k_{\mathrm{B}}T_e}} \quad (16)$$
$$= 2e^{\frac{e(V_{\mathrm{float}}-37/2)}{k_{\mathrm{B}}T_e}} \sinh\left(\frac{27e}{2k_{\mathrm{B}}T_e}\right) \quad (17)$$

[90] The integral I_0 will then be calculated with two methods: (1) using the full electron distribution measured by CAPS ELS or (2) assuming a Maxwellian distribution and using the electron moments n_e and T_e provided by the same

instrument (see section 2.3.1 for more details about the CAPS ELS data).

[91] If we choose the full measured distribution, we have first to transform the initial differential number fluxes $F(E)$ $((\mathrm{keV\,cm}^2\,\mathrm{sr\,s})^{-1})$ measured in each of the 64 energy channels into the distribution function f_{ie} $(s^3 m^{-6})$:

$$f_{\mathrm{ie}}(E) \sim \frac{5 m_e^2 F(E)}{eE} \quad (18)$$

[92] The integral I_0 is then calculated numerically from the knowledge of the differential number fluxes measured by CAPS ELS.

[93] If we choose the method based on the electron moments n_e and T_e, as well as the SEEY function by *Sanders and Inouye* [1978], then the integral I_0 may be calculated analytically (see Appendix A):

$$I_0 = n_e K L \quad (19)$$

with

$$K = \sqrt{\frac{k_{\mathrm{B}}T_e}{2\pi m_e}}\,A_{\mathrm{LP}}e \quad (20)$$

$$L = 1 - \eta_e + \frac{cb^2}{(b + k_{\mathrm{B}}T_e)^2} - \frac{ca^2}{(a + k_{\mathrm{B}}T_e)^2} \quad (21)$$

[94] The final expressions for b_{ener} are, respectively, for the full ELS distribution and a Maxwellian distribution:

$$\begin{cases} b_{\mathrm{ener_{full}}} = -\frac{10\pi A_{\mathrm{LP}} A}{27} \int_0^\infty F(E)(1 - \delta_e(E) - \eta_e(E))\mathrm{d}E \\ b_{\mathrm{ener_{maxw}}} = -\frac{A n_e K L}{27} \end{cases} \quad (22)$$

5.1.3.2. The I_{ener} Contribution

[95] The initial DC level m of the current-voltage curve is defined by

$$m = \frac{\int_{U_{\mathrm{B}}=-5}^{U_{\mathrm{B}}=-32}(I_-(U_{\mathrm{B}}) + bU_{\mathrm{B}})\mathrm{d}U_{\mathrm{B}}}{27} \quad (23)$$

[96] The I_{ener} contribution to the DC level of the current-voltage curve of the LP is thus given by

$$I_{\mathrm{ener}} = \frac{\int_{U_{\mathrm{B}}=-32}^{U_{\mathrm{B}}=-5}(I_{\mathrm{energet}}(U_{\mathrm{B}}) + b_{\mathrm{ener}}U_{\mathrm{B}})\mathrm{d}U_{\mathrm{B}}}{27} \quad (24)$$

which leads to

$$I_{\mathrm{ener}} = \frac{I_0 \int_{U_{\mathrm{B}}=-32}^{U_{\mathrm{B}}=-5}(e^{\frac{e(V_{\mathrm{float}}+U_{\mathrm{B}})}{k_{\mathrm{B}}T_e}} - AU_{\mathrm{B}}/27)\mathrm{d}U_{\mathrm{B}}}{27} \quad (25)$$

leading, using the parameters I_0 and A, to

$$I_{\mathrm{ener}} = \frac{AI_0(\frac{k_{\mathrm{B}}T_e}{e} - 37/2)}{27} \quad (26)$$

[97] The calculation of I_0 (see previous section and Appendix A) gives the following final expressions for I_{ener}, respectively, for the full ELS distribution and a Maxwellian distribution:

$$\begin{cases} I_{\mathrm{ener_{full}}} = -\frac{10\pi A_{\mathrm{LP}} A(\frac{k_{\mathrm{B}}T_e}{e}-37/2)}{27} \int_0^\infty F(E)(1 - \delta_e(E) - \eta_e(E))\mathrm{d}E \\ I_{\mathrm{ener_{maxw}}} = -\frac{A n_e K L(\frac{k_{\mathrm{B}}T_e}{e}-37/2)}{27} \end{cases} \quad (27)$$
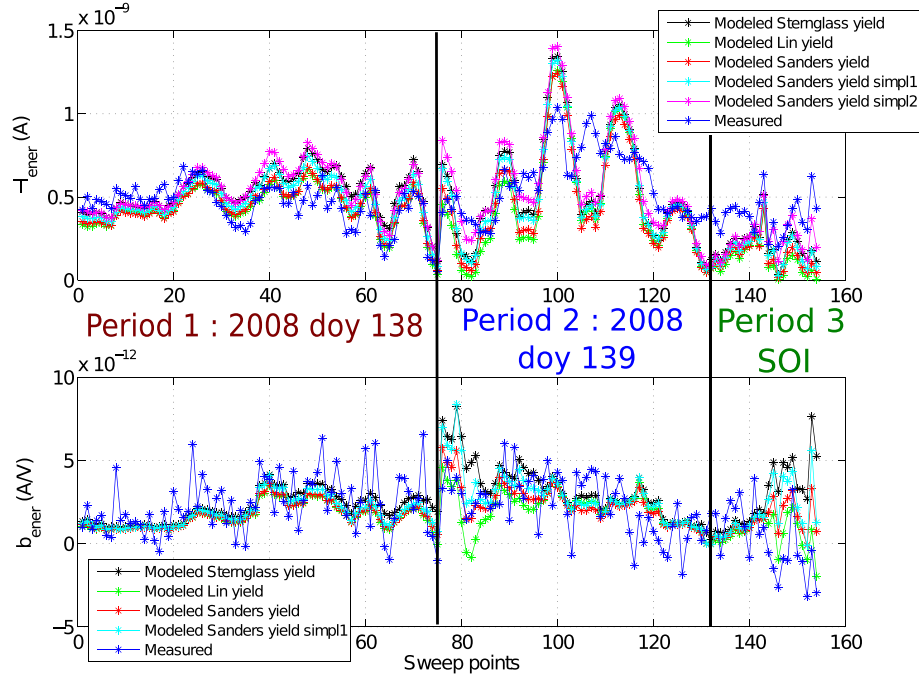
Figure 10. (top) $-I_{ener}$ and (bottom) b_{ener} measured and modeled with the full distribution method during the case studies (inbound and outbound legs of the high-inclination orbit, SOI). The modeled values use several SEEY functions [*Sternglass*, 1957; *Lin and Joy*, 2005; *Sanders and Inouye*, 1978] as well several levels of simplifications for the expressions of I_{ener}/b_{ener} ("simpl1"/"simpl2" refer to the first/second simplification level). See the text for more details.

5.1.3.3. Simplified Expressions

[98] The expressions for b_{ener} and I_{ener} developed in the previous sections need the knowledge of several information: the electron distribution (in particular the electron temperature T_e derived after a complex analysis of the CAPS ELS data), the secondary and backscattering coefficients, and also the floating potential V_{float}. V_{float} is derived from an independent and nonautomatic analysis of the electron side (positive potential U) of the LP current-voltage curve.

[99] If we want to remove the parasite contribution due to the energetic electrons from the LP observations during the Cassini mission, the search of easy and automatic calculations should be investigated. Two levels of simplification may be used to derive expressions needing less input parameters.

[100] If we focus on the regions where the electron temperature is large, and given the low absolute values of the potential V_{float} (e.g., $-1.1 < V_{float} < +0.5$ V during the case studies), the expression of the parameter A may be simplified to remove V_{float}. For low ratios $\frac{e(V_{float}-37/2)}{k_B T_e}$, we have

$$A \sim \frac{27e}{k_B T_e} \qquad (28)$$

[101] One then directly replaces A by this approximation into the equations for b_{ener} (22) and I_{ener} (27) to obtain the simplified parameters $b_{ener_{sim}}$ and $I_{ener_{sim}}$ where V_{float} is not present anymore.

[102] A second level of simplification can be applied to the calculation of I_{ener} in order to remove both the electron temperature and the floating potential. If we again consider large enough temperatures, the ratio $\frac{\frac{k_B T_e}{e}-37/2}{\frac{k_B T_e}{e}} \to 1$,

so that equation (26) (combined with equation (28)) simply becomes

$$I_{ener} \sim I_{ener_{simpl2}} = I_0 \qquad (29)$$

[103] This simplification allows, when using the full measured distribution instead of the electron moments, to approximate I_{ener} with the only use of the CAPS ELS flux distribution measured.

[104] The first approximation induces an error between 4.0/3.7% and 21.3/19.4% for V_{float} between -1.1 and $+0.5$ V and for $T_e = 100/500$ eV. The second simplification induces in the end an error of 49/21/8% for $T_e = 100/200/500$ eV and $|V_{float}| < 1$ V.

[105] The influence of the simplification levels will be discussed in the next section and shown in Figures 10 and 11. In the absence of additional information, the exact expressions were always used in the paper to obtain more rigorous results.

5.2. Comparison With the Observations During the Case Studies

[106] In this section, we will compare the modeled and measured I_{ener} and b_{ener} contributions during the case studies by using maximum yield values derived later in section 5.3.1.

[107] Figure 10 shows the resulting comparison between the modeled and measured values of I_{ener} and b_{ener} for the full distribution method (defined in section 2.3.1.1). The maximum yield values $\delta_{e_{max}}$ used for both parameters were, respectively, 3.6 and 3.2 (see section 5.3.1 and Table 1). The figure shows the modeled parameters for several levels of simplifications (see section 5.1.3.3 for their description),
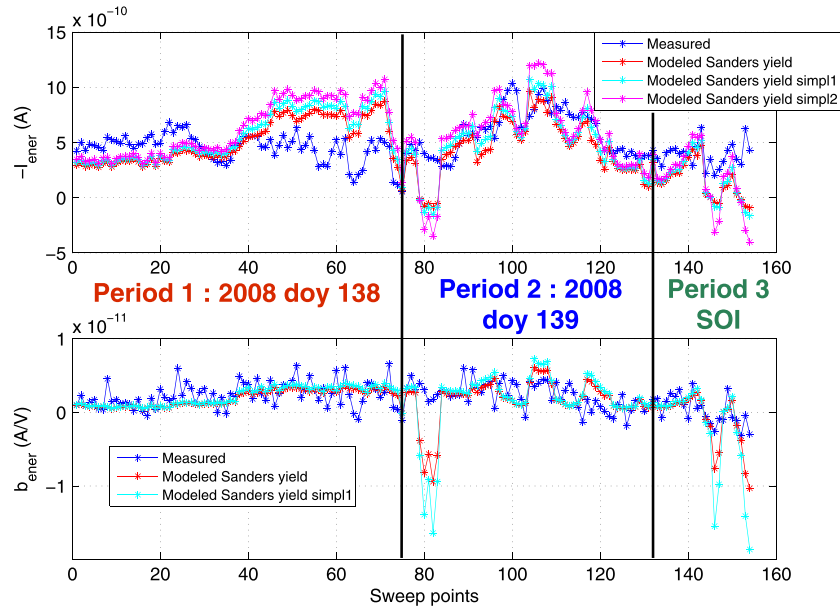
Figure 11. (top) $-I_{ener}$ and (bottom) b_{ener} measured and modeled with the moments method during the case studies (inbound and outbound legs of the high-inclination orbit, SOI). Several levels of simplification for the expressions of I_{ener}/b_{ener} are compared ("simpl1"/"simpl2" refer to the first/second simplification level). See the text for more details.

i.e., two levels of simplification for I_{ener} and one for b_{ener}. Moreover, the influence of the choice of the SEEY function is shown, with a comparison between the three references detailed in section 5.1.2.1.

[108] The relative errors (after a quartile filtering) between the measured and modeled parameters are of the same order for any yield function or simplification level: ~ 27–33% for I_{ener} and ~ 53–62% for b_{ener}. There is a few percent increased error for simplified expressions compared with the exact formula and a minimum error for the yield function given by *Sanders and Inouye* [1978]. Moreover, the DC level is better reproduced than the slope of the current-voltage curve due to the dynamic profile of the measured slope (as discussed in section 4.3).

[109] Figure 11 shows the same comparison for the moments method (defined in section 2.3.1.3). The maxi-

mum yield values $\delta_{e_{max}}$ used were 1.3 and 1.15, respectively, for I_{ener} and b_{ener} (see section 5.3.1 and Table 1). The figure shows the modeled parameters for several levels of simplifications and the *Sanders and Inouye* [1978] SEEY function.

[110] The relative errors (after a quartile filtering) are of the same order as for the full distribution method, though slightly enhanced, with ~ 36–40% for I_{ener} and ~ 57–63% for b_{ener}. The exact expressions and the DC level still give the best results.

[111] The two figures, however, show significant errors at some time intervals of the case studies. In particular, the full distribution method is not always efficient during periods 2 and 3, and the moments method is not appropriate during the beginning of period 2 and during a part of period 3. These large errors may be explained by two main problems. First,

Table 1. Comparison Between the Different Methods to Reproduce the I_{ener} and b_{ener} Contributions During the Case Studies[a]

	Rel. error Inb. (%)	$\delta_{e_{max}}$ Inb.	Rel. error Inb.-Outb. (%)	$\delta_{e_{max}}$ Inb.-Outb.	Rel. error all periods (%)	$\delta_{e_{max}}$ all periods
I_{ener}						
Statistical method selection 1	14/12	n/a	14/13	n/a	16/15	n/a
Statistical method selection 2	13/12	n/a	13/13	n/a	15/14	n/a
Full CAPS ELS distribution	18/16	3.65/3.75	21/20	3.6/3.6	27/25	3.6/3.6
Electron moments	39/38	1.3/1.3	33/33	1.3/1.3	36/26	1.3/1.3
b_{ener}						
Statistical method selection 1	49/69	n/a	57/75	n/a	66/80	n/a
Statistical method selection 2	47/59	n/a	54/63	n/a	60/72	n/a
Full CAPS ELS distribution	40/53	3.45/3	44/55	3.25/3	55/62	3.2/3
Electron moments	49/58	1.15/1.1	53/65	1.15/1.1	58/77	1.15/1.1

[a]The statistical method (section 4.1) uses fit functions based on the analysis of two initial different data selections (shown in Figure 5) whereas the theoretical approach (section 5.1.3) uses either the full electron distribution measured or the derived electron moments. The relative errors between the measurements and modeling are given in percent after a quartile filtering. The best values for the maximum yield $\delta_{e_{max}}$ are given for the moments and full distribution methods (see section 5.3.1). The values with/without correction (e.g., "14/12") for the thermal ion contribution (I_{ions}) are compared in each cell. "Inb." refers to 17 May 2008 at 19:30–20:10 UT; "Inb.-Outb." refers to both 17 May 2008 at 19:30–20:10 UT and 18 May 2008 at 1:40–2:10 UT; "all periods" refers to 17 and 18 May 2008 as well as SOI (30 June 2004 at 16:00–20:00 UT).
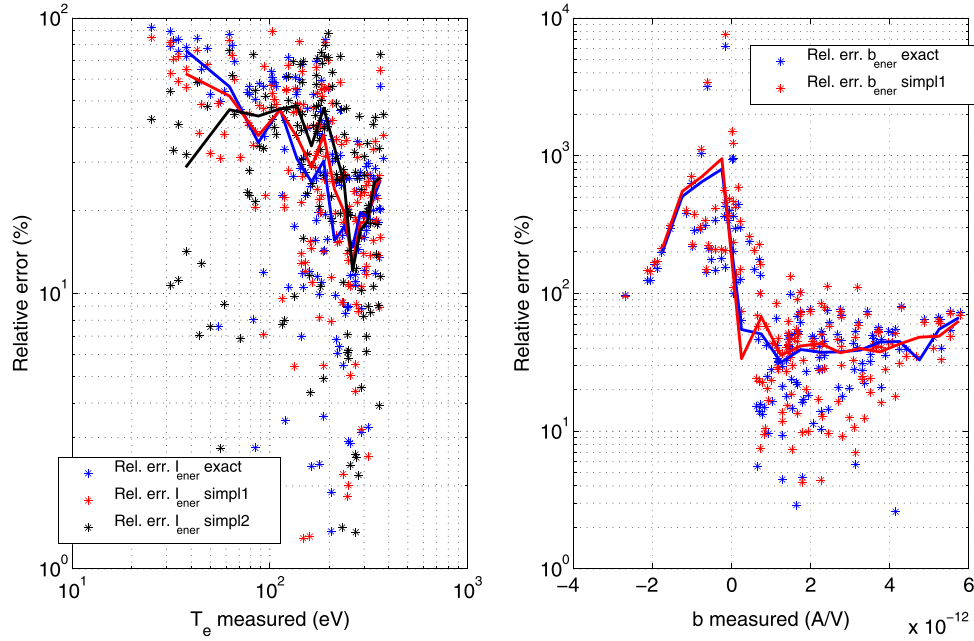
Figure 12. Relative error during the case studies between the measured and modeled values ($\frac{|\text{meas.}-\text{model.}|}{\text{meas.}}$ in percent) of (left) I_{ener} as a function of the measured incident electron temperature and (right) b_{ener} as a function of the measured slope b. Several levels of simplification are compared, and the mean profile for each data set is shown (solid line).

when the spacecraft is rotating, e.g., during period 2, this induces a variable pitch angle coverage for anode 5 used by the CAPS ELS instrument. This may lead to strong associated variations of the electron data which are then visible in our modeling. Second, when the electron temperature is too low (e.g., < 100 eV), as was the case during a part of period 3 or at the beginning of period 2, the influence of the energetic electrons is more difficult to investigate and model (as discussed in section 3.2).

[112] Figure 12 gives the relative errors between measurements and modeling of the energetic contributions, as a function of the electron temperature (Figure 12, left) and of the slope b of the I-V curve (Figure 12, right). Figure 12 (left) thus demonstrates the limit related to the electron temperature of the incident plasma: the relative errors for the I_{ener} contribution strongly decrease at electron temperatures above 100 eV. Section 4.2 also showed how the (positive) values of the slope b could be used to identify the regions influenced by the energetic electrons and thus where the modeling of $I_{\text{ener}}/b_{\text{ener}}$ should be the most efficient. Figure 12 (right) confirms that the modeling errors (here for b_{ener}) are reduced for positive—and large—slope values. Both dependencies are obviously related, since the large positive slope values are generated by incident plasmas with $T_e \in [T_A; T_*]$ (see Figure 4).

[113] A global comparison between the full distribution and moments methods will be given in section 6.

5.3. Deriving the Maximum Secondary Electron Yield Value for the LP Surface

[114] In this section, we will investigate the best value of the maximum yield $\delta_{e_{\max}}$ to be used for the LP surface. The $\delta_{e_{\max}}$ values used in section 5.2 were derived from the calculations detailed in section 5.3.1. Moreover, these derived

values will be compared with another method (section 5.3.2) based on the knowledge of the anticritical temperature of the LP surface [*Lai and Tautz*, 2008]. They will also be compared with laboratory measurements described in the literature for similar surface compositions (section 5.3.3).

5.3.1. Derivation From the Comparison Between Modeling and Measurements

[115] The comparison between the modeled $I_{\text{ener}}/b_{\text{ener}}$ contributions and the observed values may be used through two different ways: one allowing to derive the best $\delta_{e_{\max}}$ for each time interval, and one to derive the best value for a specific data set.

[116] The first method is based on the fact that the SEEY functions detailed in section 5.1.2.1 are all directly proportional to the $\delta_{e_{\max}}$ constant parameter. It is thus possible to extract analytically the needed $\delta_{e_{\max}}$ value from equations (26) and (14) to reproduce exactly the measured values of, respectively, I_{ener} and b_{ener} at each time interval:

$$
\begin{cases}
\delta_{e_{\max}I_{\text{ener}}} = \dfrac{\frac{A(\frac{k_B T_e}{e}-37/2)}{27}\frac{2\pi e}{m_e^2}A_{\text{LP}}\int_0^\infty E f_{\text{ie}}(E)(1-\eta_e)\mathrm{d}E - I_{\text{ener}}}{\frac{A(\frac{k_B T_e}{e}-37/2)}{27}\frac{2\pi e}{m_e^2}A_{\text{LP}}\int_0^\infty E f_{\text{ie}}(E)\frac{\delta_e(E)}{\delta_{e_{\max}}}\mathrm{d}E} \\[2ex]
\delta_{e_{\max}b_{\text{ener}}} = \dfrac{\frac{-A}{27}\frac{2\pi e}{m_e^2}A_{\text{LP}}\int_0^\infty E f_{\text{ie}}(E)\mathrm{d}E - b_{\text{ener}}}{\frac{-A}{27}\frac{2\pi e}{m_e^2}A_{\text{LP}}\int_0^\infty E f_{\text{ie}}(E)\frac{\delta_e(E)}{\delta_{e_{\max}}}\mathrm{d}E}
\end{cases}
\tag{30}
$$

[117] Such calculations lead to the following minimum/mean/maximum values of $\delta_{e_{\max}}$ during the case studies: $\delta_{e_{\max}I_{\text{ener}}}$ = 2.90/4.12/10.17 and 0.95/1.50/4.85 for the respective full distribution and moments methods; $\delta_{e_{\max}b_{\text{ener}}}$ = −0.44/3.36/6.70 and −0.10/1.26/2.72 for the respective full distribution and moments methods. This approach thus suggests a large range of maximum yield values, with even unphysical negative values at some time intervals.
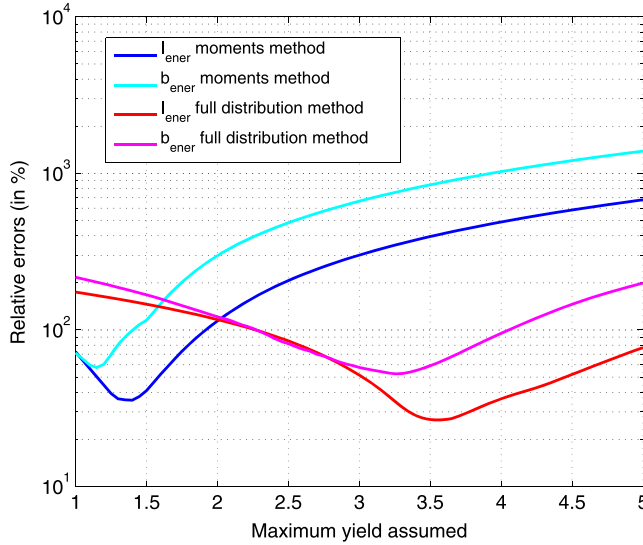
Figure 13. Relative errors (in percent; after a quartile filtering) during the three case study periods, between the measured and modeled values ($\frac{|\text{meas.}-\text{model.}|}{\text{meas.}}$) of I_{ener} and b_{ener}, as a function of the assumed maximum secondary electron yield value $\delta_{e_{\max}}$. Both the full distribution and the moments methods are compared.

[118] A second method was used, based on the minimization of the mean relative errors between the measured and modeled values of $I_{\text{ener}}/b_{\text{ener}}$ during the case studies. The corresponding $\delta_{e_{\max}}$ values were chosen in section 5.2 and are shown in Table 1. The results of this second method are shown in Figure 13, where the relative error is given as a function of the maximum yield $\delta_{e_{\max}}$ assumed for the modeling. The calculations are performed for both I_{ener} and b_{ener} as well as for both the full distribution and moments methods. A clear minimum error is obtained for each curve, at $\delta_{e_{\max}}$ values of $\sim 3.6/3.2$ or $\sim 1.3/1.15$ for $I_{\text{ener}}/b_{\text{ener}}$ using the full distribution or the moments method.

[119] A strong difference between the $\delta_{e_{\max}}$ values derived from the full distribution and moments methods thus appears, much stronger than the difference between the usage of I_{ener} and b_{ener}. This will be discussed in section 5.3.3.

[120] Moreover, the method based on the minimization of the relative errors and using the electron moments was applied to a selection of the large data set. This selection includes all LP data from 1 February 2005 to 30 July 2008 with the spacecraft located off the equator ($|Z| > 2 R_S$), with T_e in the range $[100; 500]$ eV and with large enough measured slope values ($b > 2 \times 10^{-3}$ nA/V). Such a selection—given our analysis in sections 4.2 and 3.2.2 or in Figure 12—allows us to obtain a large amount of measurements of the I_{ener} and b_{ener} contributions, despite the absence of correction for the cold ions contribution which should be negligible. The best maximum yields derived are 1.5 and 1.55 for I_{ener} and b_{ener}, respectively (see Table 2).

5.3.2. Derivation From the Knowledge of the Anticritical Temperature T_A

[121] The usage of the formalism by *Lai and Tautz* [2008] allows to derive an independent estimate of the maximum

yield value based on the knowledge of the critical and anticritical temperatures for the LP surface.

[122] Both T_A and T_* correspond indeed to an equilibrium between the incident and the secondary + backscattered electrons, i.e., to the following condition:

$$\int_0^\infty E f_{\text{ie}}(E)(1 - \delta_e(E) - \eta_e(E))\mathrm{d}E = 0 \qquad (31)$$

which leads, assuming a Maxwellian distribution for the incident electrons, the SEEY function $\delta_e(E)$ by *Sanders and Inouye* [1978], and a constant backscattering coefficient η_e, to

$$c((1 + k_B T/a)^{-2} - (1 + k_B T/b)^{-2}) + \eta_e = 1 \qquad (32)$$

Since $c = 1.37\delta_{e_{\max}}$ (see section 5.1.2.1), one can finally infer the following:

$$\delta_{e_{\max}} = \frac{1 - \eta_e}{1.37((1 + k_B T/a)^{-2} - (1 + k_B T/b)^{-2})} \qquad (33)$$

[123] The introduction in this equation of the values derived in section 3.2.2 for T_A and T_*, respectively, 50–60 eV and 600–800 eV, leads to $\delta_{e_{\max}} \sim 1.22$–$1.11$ and $\delta_{e_{\max}} \sim 1.06$–$1.25$. These values are in the same range as the one derived from the minimum error analysis with a Maxwellian distribution discussed in the previous section.

[124] The peak energy of the SEEY function was always assumed constant at 350 eV in this work, based on our previous work (G12). The peak energy is, however, not very precisely known. Considering a peak energy in a range such as 300–400 eV would lead to a broader range for $\delta_{e_{\max}}$ of $[1.00; 1.39]$.

5.3.3. Comparison With Laboratory Measurements

[125] The $\delta_{e_{\max}}$ value was considered at first as unknown in this paper, since the maximum secondary yield strongly depends on the exact surface composition and treatment (heating, cleaning, etc.). No laboratory measurements were indeed performed for the Cassini LP surface. However, laboratory measurements may be found in the literature for similar surfaces [*Baglin et al.*, 2000; *He et al.*, 2001; *Walters and Ma*, 2001; *Lorkiewicz et al.*, 2007]. These authors propose a broad range of possible maximum yield values, between 1.1 and 2.4.

[126] The literature does not provide a precise value for $\delta_{e_{\max}}$. However, it provides a range that is in agreement with the values derived in the previous sections (see Tables 1

Table 2. Same as Table 1 for All LP Data From 1 February 2005 to 30 July 2008 off the Equator ($|Z| > 2 R_S$), in the Incident Electron Temperature Range $T_e = [100; 500]$ eV and With Large Enough Slope Values ($b > 2 \times 10^{-3}$ nA/V)[a]

	Rel. error (%)	Correlation factor	$\delta_{e_{\max}}$
I_{ener}			
Statistical method selection 1	23	0.72	n/a
Statistical method selection 2	24	0.74	n/a
Electron moments	40	0.61	1.5
b_{ener}			
Statistical method selection 1	37	0.52	n/a
Statistical method selection 2	41	0.60	n/a
Electron moments	40	0.53	1.55

[a]The Pearson's correlation factor [*Press et al.*, 2007] is given along with the relative error in percent (no quartile filtering was applied). No correction was performed to remove the thermal ion contribution (I_{ions}).

and 2), except for the full distribution method where $\delta_{e_{\max}} \geq$ 3.2. A detailed investigation was performed to check for possible errors inducing such large unrealistic maximum yield values with the full distribution method. We thus tested the sensitivity of the results to parameters such as the method of integration, the choice of the CAPS anode or time averaging, a variation of the floating potential, the method of interpolation toward the LP time intervals, or the choice of the exact peak energy of the SEEY function. Such tests, however, only lead to relative changes below 10% for the $\delta_{e_{\max}}$ value.

[127] The theoretical approach used in this paper, based on the work by *Lai et al.* [1983], should in principle be compatible with any incident electron distribution function $f_{ie}(E)$. However, the Boltzmann reduction factor used in this approach (i.e., $e^{\frac{eU}{k_B T_e}}$, see equation (10)), which allows to simplify the influence of the surface potential, is essentially correct for a Maxwellian distribution. This factor corresponds indeed to a shift in energy for incident Maxwellian electrons due to the potential U of the surface: $f_{\mathrm{maxw}}(E+eU) = f_{\mathrm{maxw}}(E)e^{\frac{eU}{k_B T_e}}$.

[128] The *Lai et al.* [1983] approach is thus probably not fully appropriate for non-Maxwellian distributions: despite a good correspondence between the measured and modeled I_{ener} and b_{ener} contributions, an unrealistic maximum yield value is needed.

6. Comparison Between the Various Modeling Methods

6.1. The Precision of the Modeling Methods

[129] Tables 1 and 2 show the comparison between the three methods developed to reproduce the observed contributions of the incident energetic electrons to the respective DC level (via I_{ener}) and slope (via b_{ener}) of the current-voltage curve. The three methods are as follows: (1) an empirical statistical fit (initially performed on the large data sets "selection 1" and "selection 2") as a function of the 253–474 eV incident electron differential number flux measured by CAPS ELS (see section 4.1 and Figure 8), (2) a theoretical approach using the full (with all energy channels) incident electron distribution measured (see section 5 and Figure 10), and (3) the same theoretical approach using the incident electron moments (see section 5 and Figure 11).

[130] The relative errors and best maximum yield values are derived from a minimization of the errors between the measurements and the modeling (see section 5.3.1).

[131] Table 1 shows the results for the case studies. For comparison, we provide the results when the minimization is performed for the following: the three case study periods together (as previously discussed in the paper; rightmost columns), but also for the inbound leg of the high-inclination event only (leftmost columns), or for both inbound/outbound legs of this event (columns in the center). The results are also given with and without correction for the contribution by the cold ions. The following conclusions can be given for the case studies:

[132] 1. For modeling I_{ener}, the statistical approach provides the smallest errors, followed by the full distribution and the electron moments methods; all methods are roughly similar for modeling b_{ener}, with slightly better results for the full distribution method.

[133] 2. I_{ener} is better reproduced than b_{ener} in all cases.

[134] 3. The influence of the correction due to the cold ions is small for I_{ener} (+6% error variation on average) and reasonable for b_{ener} (–16%); the choice of the exact data set used among the case study periods has no strong impact, as also the choice of the initial selection for the fit functions of the statistical approach.

[135] 4. The maximum yield values are very stable, with strong differences only between the electron moments and full distribution methods (discussed in section 5.3.3).

[136] Table 2 corresponds to a larger data set (1200 h of data) based on several criteria regarding the location of the spacecraft (the least important, since mostly redundant with the next two criteria), the value of the slope measured by the LP, and the incident electron temperature. This selection allows to focus on a large number of time intervals where the influence of the energetic electrons is the strongest. The influence may even be stronger than during some parts of the case study periods where all these criteria were not encountered together. The resulting minimization process leads to larger values for the maximum yield than based on the case studies, and smaller relative errors (similar error values are obtained but without any quartile filtering of the data). The relative errors are similar (at $\sim 40\%$) for all methods except for I_{ener} with the statistical approach where it is smaller.

6.2. The Limits of the Modeling Methods

[137] Beyond the error with respect to the measurements, each method suffers from specific limits:

[138] 1. The statistical approach is only empirical and thus can hardly be used directly in other contexts (e.g., other magnetospheres, other LP surface compositions); the flux thresholds and fit functions derived also depend on the data set selection criteria used; moreover, the statistical approach does not allow to understand the physics behind the observations.

[139] 2. The full distribution method uses unrealistic values of the maximum secondary yield; the usage of a more complex and detailed approach (including the rigorous influence of the surface potential and eventually sheath effects) is needed to take into account the full incident electron distribution measured in the equations.

[140] 3. The moments method assumes a complex derivation process of the electron moments from the raw counts measured, which makes difficult any automatic calculation to remove the I_{ener} and b_{ener} contributions to the LP measurements; this method is also limited in the presence of strongly non-Maxwellian incident plasmas.

[141] Moreover, all methods suffer from the following:

[142] 1. One is the absence of precise values of the maximum yield and backscattering coefficient for the exact LP surface composition and treatment; their strong impact on the modeling underlines the need of such future laboratory measurements.

[143] 2. Another is the low level of the slope b of the current-voltage curve in such low-density regions of the magnetosphere.

[144] 3. Next is the complexity of the physics of the interaction between the LP surface and the incident plasma, which would need a more rigorous derivation of the currents measured; this derivation would, however, probably make any calculation too complex to allow an efficient and

automatic removal of the I_{ener} and b_{ener} contributions from the LP measurements.

[145] 4. Last is the complex combination of the data sets from two different instruments, i.e., the LP and CAPS ELS instruments: each has its own uncertainties, different locations on the spacecraft (inducing slightly different impacting plasmas), and different temporal resolutions (which need an interpolation process leading to possible errors); in particular, the influence of the spacecraft itself, through the eventual blockage of a part of the incident electrons (in a specific way for each instrument), is not taken into account and would need detailed and complex simulations that are beyond the scope of the paper.

[146] Despite all the limits mentioned, we have shown that the influence of the energetic electrons on the LP observations may be modeled with a reasonable precision via several methods. These methods—in particular the statistical and moments methods which need easy calculations—may be used through the whole Cassini mission to remove automatically the contribution to the full current-voltage curve or to the derived DC level and slope parameters.

7. Summary

[147] This paper further investigates a previous work [*Garnier et al.*, 2012b], which showed evidence for a strong sensitivity of the Cassini Langmuir Probe measurements to the energetic (i.e., ~ 250–450 eV) electrons at Saturn. These energetic electrons impact the surface of the probe and generate a current of secondary electrons. *Garnier et al.* [2012b] demonstrated that this induces an energetic contribution I_{ener} to the DC level of the current-voltage curve measured by the LP.

[148] In this paper, we have done the following:

[149] 1. We showed how the secondary electrons not only impact the DC level of the current-voltage curve (through the added contribution I_{ener}) but also impact the slope of this curve (through an added contribution b_{ener}); unexpected positive slope values were also revealed.

[150] 2. We explained how the slope of the current-voltage curve can be used to clearly identify when the influence of the energetic electrons is strong on the LP observations.

[151] 3. We interpreted the influence of the energetic electrons in terms of the critical and anticritical temperatures concept detailed by *Lai and Tautz* [2008] for spacecraft surfaces; we thus provided the first observational evidence for the existence of the anticritical temperatures; these two temperature values were also identified, respectively, at ~ 50–60 eV and ~ 600–800 eV.

[152] 4. We managed to model, with a reasonable precision ($\sim 40\%$ error on average), the energetic contributions I_{ener} and b_{ener} via several methods: (1) an empirical statistical fit as a function of the 253–474 eV incident electron differential number flux measured by the CAPS ELS instrument, (2) a theoretical approach using the full—with all energy channels—incident electron distribution measured, and (3) the same theoretical approach using the incident electron moments measured.

[153] 5. We were able to derive indirect estimations of the maximum secondary yield value for the LP surface from measurements performed onboard a spacecraft (instead of laboratory measurements).

[154] 6. We proposed an approach to understand the influence of the energetic electrons on the measurements of a Langmuir probe; this approach can be used in other contexts than the Cassini LP at Saturn, such as the future missions Jupiter Icy Moons Explorer at Jupiter, BepiColombo at Mercury, Rosetta at the comet Churyumov-Gerasimenko, and even the probes onboard spacecrafts launched in the Earth magnetosphere.

[155] Further work should be done to evaluate the impact of the energetic electrons influence on previous Langmuir probe studies. However, the magnetospheric regions concerned are usually not investigated (except in large scale analysis such as the Saturn Orbit Insertion analysis by *Wahlund et al.* [2005b]), since they are expected to generate mostly a photoelectron current. Thus, photoelectron current analysis could be impacted, as well as eventually studies of the highest ionospheric altitudes or of hot plasma beams in the ionospheres.

[156] Future investigations should also be performed to ameliorate the understanding of the influence of the energetic particles. Laboratory measurements of the secondary emission yield (energy and angular) function should be done for the exact Cassini LP surface composition and treatment. More rigorous expressions could be derived to model the energetic electrons influence based on the full incident electron distribution function measured. Several perspectives also arise for the near future from our work. One can remove, for the whole Cassini mission, the influence by the energetic electrons from the LP measurements. A future paper will also show how we can conversely derive useful information about the energetic electrons from this influence.

Appendix A: Deriving the I_{ener} and b_{ener} Contributions for a Maxwellian Electron Distribution Function

[157] The I_{ener} and b_{ener} contributions are, respectively, given by (equations (26) and (14)):

$$\begin{cases} I_{\text{ener}} = \frac{AI_0(\frac{k_B T_e}{e}-37/2)}{27} \\ b_{\text{ener}} = -I_0 A \end{cases} \quad (A1)$$

with

$$I_0 = \frac{2\pi e}{m_e^2} A_{\text{LP}} \left(\int_0^\infty E f_{\text{ie}}(E)(1-\delta_e(E)-\eta_e(E))\mathrm{d}E \right) \quad (A2)$$

and (sinh hyperbolic sinus function)

$$A = \frac{2}{27} e^{\frac{e(V_{\text{float}}-37/2)}{k_B T_e}} \sinh(\frac{27e}{2k_B T_e}) \quad (A3)$$

[158] We will consider in this appendix the case for an incident Maxwellian electron distribution function:

$$f_{\text{ie}} = n_e \left(\frac{m_e}{2\pi k_B T_e}\right)^{3/2} e^{-\frac{E}{k_B T_e}} \quad (A4)$$

[159] The integral I_0 becomes, for a constant η_e and for $\delta_e(E)$ given by *Sanders and Inouye* [1978]

$$I_0 = \frac{2\pi e}{m_e^2} A_{\text{LP}} n_e \left(\frac{m_e}{2\pi k_B T_e}\right)^{3/2} *$$
$$\int_0^\infty E e^{-\frac{E}{k_B T_e}} (1-\eta_e - ce^{-E/a} + ce^{-E/b})\mathrm{d}E \quad (A5)$$

$$I_0 = \frac{2\pi e}{m_e^2} A_{\text{LP}} n_e \left(\frac{m_e}{2\pi k_B T_e}\right)^{3/2} \int_0^\infty E \left(e^{-\frac{E}{k_B T e}}(1-\eta_e)\right.$$
$$\left. - ce^{-E(1/(k_B Te)+1/a)} + ce^{-E(1/(k_B Te)+1/b)}\right)\mathrm{d}E$$
$$\text{(A6)}$$

which may be written as

$$I_0 = C(I_1 + I_2) \tag{A7}$$

with

$$C = \frac{2\pi e}{m_e^2} A_{\text{LP}} n_e \left(\frac{m_e}{2\pi k_B T_e}\right)^{3/2} \tag{A8}$$

$$I_1 = (1-\eta_e) \int_0^\infty E e^{-\frac{E}{k_B T e}} \, \mathrm{d}E \tag{A9}$$

$$I_2 = \int_0^\infty -cE(e^{-E(1/(k_B Te)+1/a)} - e^{-E(1/(k_B Te)+1/b)})\mathrm{d}E \tag{A10}$$

Then using

$$\int_0^\infty E e^{-\frac{E}{x}} \, \mathrm{d}E = x^2 \tag{A11}$$

leads to

$$I_1 = (1-\eta_e)(k_B T_e)^2 \tag{A12}$$

and

$$I_2 = c(k_B T_e)^2 \left(\frac{b^2}{(b+k_B T_e)^2} - \frac{a^2}{(a+k_B T_e)^2}\right) \tag{A13}$$

and thus I_0 is given by

$$I_0 = C(k_B T_e)^2 \left(1 - \eta_e + \frac{cb^2}{(b+k_B T_e)^2} - \frac{ca^2}{(a+k_B T_e)^2}\right) \tag{A14}$$

The following simple expression will be used for I_0

$$I_0 = n_e KL \tag{A15}$$

with

$$K = \sqrt{\frac{k_B T_e}{2\pi m_e}} A_{\text{LP}} e \tag{A16}$$

$$L = 1 - \eta_e + \frac{cb^2}{(b+k_B T_e)^2} - \frac{ca^2}{(a+k_B T_e)^2} \tag{A17}$$

The final expressions for a Maxwellian electron distribution function are as follows:

$$\begin{cases} I_{\text{ener}} = \frac{A n_e KL \left(\frac{k_B T_e}{e} - 37/2\right)}{27} \\ b_{\text{ener}} = -A n_e KL \end{cases} \tag{A18}$$

References

Ågren, K., et al. (2007), On magnetospheric electron impact ionisation and dynamics in Titan's ram-side and polar ionosphere—A Cassini case study, *Ann. Geophys.*, *25*, 2359–2369, doi:10.5194/angeo-25-2359-2007.

Arridge, C., L. Gilbert, G. Lewis, E. Sittler, G. Jones, D. Kataria, A. Coates, and D. Young (2009), The effect of spacecraft radiation sources on electron moments from the Cassini CAPS electron spectrometer, *Planet. Space Sci.*, *57*, 854–869, doi:10.1016/j.pss.2009.02.011.

Baglin, V., J. Bojko, O. Grbner, B. Henrist, N. Hilleret, C. Scheuerlein, and M. Taborelli (2000), The secondary electron yield of technical materials and its variation with surface treatments, paper presented at Proceedings of 7th European Particle Accelerator Conference, Vienna, Austria, 217–221.

DeForest, S. (1972), Spacecraft charging at synchronous orbit, *J. Geophys. Res.*, *77*, 651–659, doi:10.1029/JA077i004p00651.

DeJong, A., J. Burch, J. Goldstein, A. Coates, and F. Crary (2011), Day-night asymmetries of low-energy electrons in Saturn's inner magnetosphere, *Geophys. Res. Lett.*, *38*, L08106, doi:10.1029/2011GL047308.

Edberg, N., et al. (2011), Structured ionospheric outflow during the Cassini T55–T59 Titan flybys, *Planet. Space Sci.*, *59*, 788–797, doi:10.1016/j.pss.2011.03.007.

Fahleson, U., C.-G. Fälthammar, and A. Pedersen (1974), Ionospheric temperature and density measurements by means of spherical double probes, *Planet. Space Sci.*, *22*, 41–66, doi:10.1016/0032-0633(74)90122-6.

Garnier, P., et al. (2009), Titan's ionosphere in the magnetosheath: Cassini RPWS results during the T32 flyby, *Ann. Geophys*, *27*, 4257–4272, doi:10.1029/2011JA017298.

Garnier, P., et al. (2012b), The detection of energetic electrons with the Cassini Langmuir probe at Saturn, *J. Geophys. Res.*, *117*, A10202, doi:10.1029/2011JA017298.

Gurnett, D., et al. (2004), The Cassini radio and plasma wave investigation, *Space Sci. Rev.*, *114*, 395–463, doi:10.1007/s11214-004-1434-0.

Gustafsson, G., and J.-E. Wahlund (2010), Electron temperatures in Saturn's plasma disc, *Planet. Space Sci.*, *58*, 1018–1025, doi:10.1016/j.pss.2010.03.007.

Hastings, D., and H. Garrett (1996), *Spacecraft-Environment Interactions*, pp. 148–152, Cambridge Univ. Press, Cambridge, U. K.

He, P., H. C. Hseuh, M. Mapes, R. Todd, and D. Weiss (2001), Development of titanium nitride coating for SNS ring vacuum chambers, paper presented at Proceedings of the 2001 IEEE Particle Accelerator Conference, Chicago, 2159–2161.

Holmberg, M., J.-E. Wahlund, and M. Morooka (2012), Ion densities and velocities in the inner plasma torus of Saturn, *Planet. Space Sci.*, *73*, 151–160, doi:10.1016/j.pss.2012.09.016.

Laframboise, J. G., R. Godard, and M. Kamitsuma (1982), Multiple floating potentials, "threshold-temperature" effects, and "barrier" effects in high-voltage charging of exposed surfaces in spacecraft, in *Proceedings of International Symposium on Spacecraft Materials in Space Environment,* Toulouse, France, ESA Report ESA-178, pp. 269–275, Eur. Space Agency Spec. Publ., Noorwijk, The Netherlands.

Lai, S. T., and M. Tautz (2006), High-level spacecraft charging in eclipse at geosynchronous altitudes: A statistical study, *J. Geophys. Res.*, *111*, A09201, doi:10.1029/2004JA010733.

Lai, S. T., and M. Tautz (2008), On the anticritical temperature for spacecraft charging, *J. Geophys. Res.*, *113*, A11211, doi:10.1029/2008JA013161.

Lai, S. T., M. S. Gussenhoven, and H. A. Cohen (1983), The concepts of critical temperature and energy cutoff of ambient electrons in high-voltage charging of spacecrafts, in *Spacecraft/ Plasma Interactions and Their Influence on Field and Particle Measurements,* Toulouse, France, ESA Report, ESA SP-198, edited by A. Pedersen, D. Guyenne, and J. Hunt, pp. 169–175, Eur. Space Agency Spec. Publ., Noorwijk, The Netherlands.

Lewis, G., N. Andre, C. Arridge, A. Coates, L. Gilbert, D. Linder, and A. Rymer (2008), Derivation of density and temperature from the Cassini-Huygens CAPS electron spectrometer, *Planet. Space Sci.*, *56*, 901–912.

Lin, Y., and D. G. Joy (2005), A new examination of secondary electron yield data, *Surf. Interface Anal.*, *37*, 895–900, doi:10.1002/sia.2107.

Lorkiewicz, J., J. Kula, S. Pszona, J. Sobczak, and A. Bilinski (2007), Sublimation TiN coating of RF power components, paper presented at Proceedings of AIP International Conference on Research and Applications of Plasmas, Greifswald, Germany, *993*, 411–414, doi:10.1063/1.2909163.

Morooka, M. W., et al. (2009), The electron density of Saturn's magnetosphere, *Ann. Geophys.*, *27*, 2971–2991, doi:10.5194/angeo-27-2971-2009.

Morooka, M. W., et al. (2011), Dusty plasma in the vicinity of Enceladus, *J. Geophys. Res.*, *116*, A12221, doi:10.1029/2011JA017038.

Mott-Smith, H. M., and I. Langmuir (1926), The theory of collectors in gaseous discharges, *Phys. Rev.*, *28*, 727–763, doi:10.1103/PhysRev.28.727.

Nilsson, T. (2009), Modelling of Cassini Langmuir probe measurements, Master thesis report, Uppsala University. http://www.space.irfu.se/exjobb/.

Olsen, R. C. (1983), A threshold effect for spacecraft charging, *J. Geophys. Res.*, *88*, 493–4995, doi:10.1029/JA088iA01p00493.

Persoon, A., et al. (2009), A diffusive equilibrium model for the plasma density in Saturn's magnetosphere, *J. Geophys. Res.*, *114*, A04211, doi:10.1029/2008JA013912.

Press, W. H., S. A. Teukolsky, W. T. Vetterling, and B. P. Flannery (2007), *Numerical Recipes 3rd Edition: The Art of Scientific Computing,* 3 ed., Cambridge Univ. Press, Cambridge.

Prokopenko, S. M. L., and J. G. Laframboise (1980), High-voltage differential charging of geosynchronous spacecraft, *J. Geophys. Res.*, *85*, 4125–4131, doi:10.1029/JA085iA08p04125.

Sanders, N. L., and G. T. Inouye (1978), Secondary emission effects on spacecraft charging: Energy distribution consideration, in *Spacecraft*

Charging Technology 1978, edited by R. C. Finke and C. P. Pike, pp. 747–755, U.S. Air Force Geophys. Lab., Hanscom, Mass.

Sittler, E., et al. (2006), Cassini observations of Saturn's inner plasmasphere: Saturn orbit insertion results, *Planet. Space Sci.*, *54*, 1197–1210, doi:10.1016/j.pss.2006.05.038.

Sittler, E., et al. (2008), Ion and neutral sources and sinks within Saturn's inner magnetosphere: Cassini results, *Planet. Space Sci.*, *56*, 3–18, doi:10.1016/j.pss.2007.06.006.

Sternglass, E. J. (1957), Theory of secondary electron emission by high-speed ions, *Phys. Rev.*, *108*, 1–12, doi:10.1103/PhysRev.108.1.

Thomsen, M., D. Reisenfeld, D. Delapp, R. Tokar, D. Young, F. Crary, E. Sittler, M. McGraw, and J. Williams (2010), Survey of ion plasma parameters in Saturn's magnetosphere, *J. Geophys. Res.*, *115*, A10220, doi:10.1029/2010JA015267.

Tsintikidis, D., D. Gurnett, L. Granroth, S. Allendorf, and W. Kurth (1994), A revised analysis of micron-sized particles detected near Saturn by the voyager 2 plasma wave instrument, *J. Geophys. Res.*, *99*, 2261–2270, doi:10.1029/93JA02906.

Wahlund, J., et al. (2005a), Cassini measurements of cold plasma in the ionosphere of Titan, *Science*, *308*, 986–989, doi:10.1126/science.1109807.

Wahlund, J.-E., et al. (2005b), The inner magnetosphere of Saturn: Cassini RPWS cold plasma results from the first encounter, *Geophys. Res. Lett.*, *32*, L20S09, doi:10.1029/2005GL022699.

Wahlund, J.-E., et al. (2009), Detection of dusty plasma near the E-ring of Saturn, *Planet. Space Sci.*, *57*, 1795–1806, doi:10.1016/j.pss.2009.03.011.

Walters, D., and Q. Ma (2001), Secondary electron yield of a thin film coating on the APS RF cavity tuners, paper presented at Proceedings of the 2001 IEEE Particle Accelerator Conference, Chicago, 2153–2155.

Wang, Z., D. Gurnett, T. Averkamp, A. Persoon, and W. Kurth (2006), Characteristics of dust particles detected near Saturn's ring plane with the Cassini radio and plasma wave instrument, *Planet. Space Sci.*, *54*, 957–966, doi:10.1016/j.pss.2006.05.015.

Whipple, E. C (1965), *The Equilibrium Electric Potential of a Body in the Upper Atmosphere and in Inter-Planetary Space*, George Washington University, Washington D. C.

Young, D., et al. (2004), Cassini plasma spectrometer investigation, *Space Sci. Rev.*, *114*, 1–112, doi:10.1007/s11214-004-1406-4.